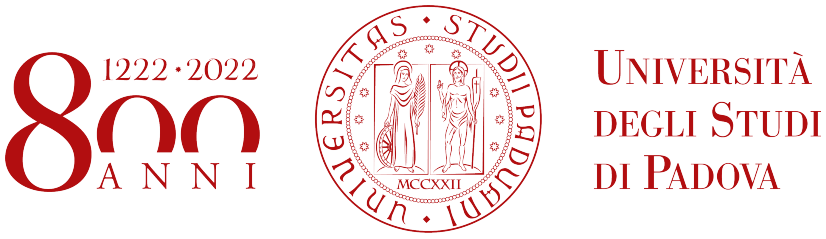

UNIVERSITÀ DEGLI STUDI DI PADOVA

Dipartimento di Ingegneria Industriale DII

Corso di Laurea Magistrale in Ingegneria Aerospaziale

Test of a gripper for autonomous in-orbit assembly with space robot

STUDENTE

Martina Imperatrice

Matricola n° 1237234

RELATORE

Dott. Branz Francesco

ANNO ACCADEMICO

2022/2023

Abstract

In recent years, the approach to both commercial and scientific space missions has been changing, and the need to reuse and renew existing resources is increasingly making its way. This happens both on the ground and in orbit, because there is a desire to reduce the development costs of a satellite, and to try to reduce the number of abandoned satellites and the growing number of space debris by space agencies and companies.

This new vision aims to make a whole series of operations to be carried out on already existing satellites become routine operations to extend their operational life. These missions are called On-Orbit Servicing (OOS) and In-Orbit Assembly (IOA).

Main servicing operation include refuelling, refurbishment, de-orbiting but also the assembling of a structure by means of modular elements.

In particular, IOA operations open up a series of nearly futuristic missions. Autonomous assembly in orbit makes it possible to go beyond the limit imposed by the launcher in terms of size and mass of the satellite, for example by allowing large astronomical observatories to be built directly in orbit, but these are not the only ones possible. Thanks to miniaturisation and the development of commercial launches, the use of small platforms is increasing. The satellites will be able to accept small auxiliary modules for power, auxiliary propulsion, telecommunication, etc.

The IOA introduces a new way of developing a satellite project which will therefore be developed from the beginning to be able to receive this type of operation. It will be necessary to study and implement a whole series of standard mechanical, power, and data exchange interfaces, which will make the concept of automatic assembly, modularity, and reuse more and more appealing.

OOS and IOA operations require the presence of two spacecraft: a chaser satellite, with one or more robotic arms, that performs servicing tasks on a target satellite. The chaser must perform a series of orbital transfer and phasing manoeuvres to allow rendezvous, initiate proximity operations, and finally execute target capture.

This phase is the most critical phase because it involves various aspects, from orbital dynamics to the development of automated capture systems. But it is also the most important phase, because once the rigid connection between the two satellites has taken place, it is possible to start the servicing operations.

The approach and capture phase is made possible by vision systems and proximity sensors that allow to control the pose of the target and the relative

distance between the two satellites.

This work continues the development of the AUTOMA project, a project founded by the Industrial Engineering department. The AUTOMA project is motivated by the high interest of the space community in IOA operations. Its purpose is to upgrade a capture system previously developed at the prototype level and to build an elementary auxiliary module to perform IOA experiments. The capture system is called SMArt Capture Kit (SMACK) and underlines the fact that it is equipped with sensors, actuators, and a computer, which makes it semi-independent from the satellite on which it is mounted. The elementary module is called Elementary Assembly Unit (EAU) and is a mock-up of an assembly module with basic functions, developed to have the standard dimensions of cube-sats.

This work gives a general overview of the parts that compose SMACK and the EAU from the mechanical point of view, of the sensors, actuators, and the navigation algorithm that estimates the pose of the target.

The work focused on the experimental tests on relative navigation sensors mounted on SMACK. These provide pose estimation and enable the autonomous assembly of modular structures and are applicable to IOA scenarios. These tests have the precise intention of evaluating the performance of the sensors chosen to have in-depth knowledge of the individual parts that make up the system. A functional test of the system was also carried out, essential for understanding the potential of SMACK, the validity of the mechanisms, and highlighting some future improvements.

Sommario

Negli ultimi anni l'approccio alle missioni spaziali sia commerciali che scientifiche è iniziato a cambiare, e si fa strada sempre più la necessità di riutilizzare e rinnovare le risorse già esistenti. Questo accade sia a terra che in orbita, perchè c'è la volontà di ridurre i costi di sviluppo di un satellite, e cercare di ridurre il numero di satelliti abbandonati e il numero di detriti spaziali crescente da parte delle agenzie spaziali e le aziende.

Questa nuova visione ha come obiettivo quello di rendere di routine tutta una serie di operazioni da effettuare su satelliti già esistenti per estenderne la vita operativa. Queste missioni prendono il nome di On-Orbit Servicing (OOS) e In-Orbit Assembly (IOA).

Le principali operazioni di servizio includono il rifornimento di carburante, il refurbishment, il de-orbiting ma anche l'assemblaggio di strutture per mezzo di elementi modulari.

Le operazione di IOA in particolare apre a una serie di missioni futuristiche. L'assemblaggio autonomo in orbita permette di oltrepassare il limite imposto dal lanciatore in termini di dimensioni e massa del satellite, ad esempio permettendo di costruire direttamente in orbita grandi osservatori astronomici, ma non è l'unica possibilità. Grazie alla miniaturizzazione e allo sviluppo di lanci commerciali, l'utilizzo di piccole piattaforme è sempre maggiore. I satelliti potranno accettare piccoli moduli ausiliari di potenza, di propulsione ausiliaria, per telecomunicazione e così via.

L'IOA introduce quindi un nuovo modo di sviluppare il progetto di un satellite, che verrà sviluppato prevedendo in partenza la possibilità di ricevere questo tipo di operazioni. Sarà necessario studiare e realizzare tutta una serie di interfacce standard di tipo meccanico, di scambio di potenza e di dati, che renderano sempre più interessante il concetto di assemblaggio automatico, modularità e riutilizzo.

Le operazioni di OOS e IOA richiedono la presenza di due satelliti: un satellite chaser, dotato di una o più braccia robotiche, che esegue operazioni di servicing su un satellite target. Il chaser deve eseguire una serie di manovre orbitali di trasferimento e di phasing per permettere il rendezvous con il satellite target, per poi iniziare le operazioni in prossimità, l'approccio finale ed infine la cattura del target.

Questa fase è la fase più critica perchè coinvolge diversi aspetti, dalla dinamica orbitale allo sviluppo di sistemi di cattura automatizzati. Ma è anche la

fase più importante, perchè una volta avvenuta la connessione rigida tra i due satelliti è possibile iniziare le operazioni di servicing.

La fase di approccio e cattura è resa possibile da sistemi di visione e sensori di prossimità che permette di controllare la posa del target e controllare la distanza relativa tra i due satelliti.

Questo lavoro porta avanti lo sviluppo del progetto AUTOMA, progetto fondato dal dipartimento di Ingegneria Industriale. Il progetto AUTOMA è motivato dall'alto interesse della comunità spaziale nelle operazioni di IOA. Ha come scopo quello di effettuare l'upgrade di un prototipo di sistema di cattura precedentemente sviluppato, e realizzare un modulo ausialiare elementare per effettuare esperimenti di IOA. Il sistema di cattura si chiama SMArt Capture Kit (SMACK) per sottolineare il fatto che è provvisto di sensori, attuatori e computer che lo rende semi-indipendente dal satellite sulla quale è montato. Il modulo elementare è chiamato Elementary Assembly Unit (EAU) ed è un mock-up di un modulo di assembly con funzioni basilari, sviluppato per avere le dimensioni standard dei cube-sat.

Questo lavoro dà una overview generale delle parti che compongono SMACK e l'EAU dal punto di vista meccanico, dei sensori, attuatori, e l'algoritmo di navigazione che stima la posa del target.

Il lavoro si è concentrato sugli esperimenti sui sensori di navigazione relativa montati su SMACK. Questi forniscono la stima della posa e consentono l'assemblaggio autonomo di strutture modulari ed è applicabile agli scenari IOA. Questi test hanno la precisa intenzione di valutare le performance dei sensori scelti per avere una conoscenza approfondita delle singole parti che compongono il sistema. Un test funzionale di sistema è stato inoltre effettuato, essenziale per comprendere le potenzialità di SMACK, la validità dei meccanismi, e mettere in luce alcuni futuri miglioramenti.

Contents

1

Introduction

1.1 On-Orbit Servicing and In-Orbit Assembly

Technological advancements in robotics and miniaturisation of systems, combined with the growth of commercial launches and the increasing usage of small platforms, lead to a new approach to space exploration. This new approach focuses on reducing satellite development costs and considering the opportunity of extending the operational life of existing satellites in orbit.

This vision is consistent with an increasing awareness of the importance, both on ground and in orbit, of the reuse and recycling of existing resources, as well as counteracting the growing number of abandoned satellites and increasing numbers of space debris.

With the On-Orbit Servicing (OOS) it is possible to satisfy this new vision. OOS missions aim to perform a series of service tasks on existing satellites to extend their capabilities and operational life. Within these services, there are also In-Orbit Assembly operations (IOA): these tasks foresee mounting a service module on already existing satellites, or the assembling of a new structure by means of modular elements.

OOS and IOA operations require the presence of two spacecraft: a chaser satellite that performs servicing tasks on a target satellite.

The chaser satellite can be a space robot (i.e. a satellite equipped with one or more robotic arms) or a satellite equipped with other types of capture systems.

Space robots have been identified as one of the most promising vehicles for performing maintenance and assembly operations [10], [21]. This is also

a consequence of the fact that the space robots can be equipped with a set of sensors and actuators which enable the automated manipulation of objects.

Potential on-orbit service operations are:

1. **Refuelling**: the chaser satellite restocks the target satellite propellant;
2. **Refurbishment**: the chaser satellite renews a component of the target satellite after malfunctions or damage caused by the space environment;
3. **Inspection**: the chaser satellite inspects the target satellite, for example to check if there are any damaged parts by means of vision systems;
4. **Orbit modification**: the chaser satellite transfers the target satellite to the correct operational orbit;
5. **Construction of large structures**: In-Orbit Assembly of large spacecraft that cannot be assembled and tested on Earth, such as large astronomical observatories, in-orbit depots, and interplanetary spaceships;
6. **Active Debris Removal and de-orbiting**: the chaser satellite captures space debris (for example, rocket upper stages) or decommissioned satellites to perform a safe atmospheric reentry or to relocate it to graveyard orbits.

These types of operation are appealing to the space industry because of the perspectives for both commercial missions and interplanetary exploration that they open. For this reason, the OOS and IOA will be increasingly investigated and researched in future space missions.

A standard OOS mission follows the next main steps [9]:

1. **Rendezvous**: is the series of actions that bring the chaser satellite to the orbit of the target satellite at a planned time and place. This is done through a series of orbital transfer and phasing manoeuvres to reduce the relative distance between the two satellites. This phase ends once the chaser satellite achieves the outer limits of a pre-defined Proximity Operations Control Volume;
2. **Close-Proximity Operations (CPOs)**: are those relative operations between the two objects within a pre-defined Proximity Operations Control Volume, where separation is typically controlled using on-board sensors to provide relative navigation;
3. **Contact Approach and Capture**: the chaser makes a final approach to the target satellite. They can make contact by various means, including docking, grappling, and netting. This phase includes three sub-phases of approach, capture and stabilisation:

(a) **Approach**: the chaser takes the final approach to the target. This approach manoeuvre uses way points in which the chaser holds position relative to the target while configuration changes or assessments are made to confirm the next step of the approach. The approach concludes once the final command is issued to initiate capture.

(b) **Capture**: there are many techniques for achieving capture, each with unique phases and subphases and associated risks. Typically, these phases will include some form of initial contact and soft capture followed by rigidization.

(c) **Post Capture Stabilisation**: the new combined vehicle is stabilised either by the chaser or by the target, or both. This phase may also include a transition period to achieve a desired servicing attitude and reconfigurations of the chaser and/or target satellite.

The major examples of OOS and IOA missions carried out so far are the construction of the International Space Station (ISS) [6] and the repair operations of the Hubble Space Telescope (HST) [11]. HST, launched in 1990, was designed for periodic servicing to maintain its operational life.

Despite these two incredible successes, space systems are not usually designed to receive this type of servicing operation. For this reason, the growth of these technologies and their use will depend on the efforts of companies and agencies towards this direction. In-depth studies of mission phases, technology demonstration missions, and standardisation of interfaces are needed.

In fact, standard mechanical, electrical, power, thermal, and data interfaces will promote reusability and encourage a more affordable exploitation of LEO, GEO, and interplanetary space. These standard interfaces will need to be interoperable, open, and modular, even if this collides with the investments of individual agencies in proprietary designs and with the associated manufacturing and supply chain interests [18].

The next section will describe some of the recent missions and near-future planned missions that investigated the opportunities offered by IOA.

1.1.1 State of the art

DARPA Phoenix Technologies The DARPA Phoenix programme's relevant study aimed at changing the traditional process of designing, developing, building, and deploying space systems, which is long, expensive, and complex. The idea was to use low-cost modular satellites (called Satlets) for autonomous IOA

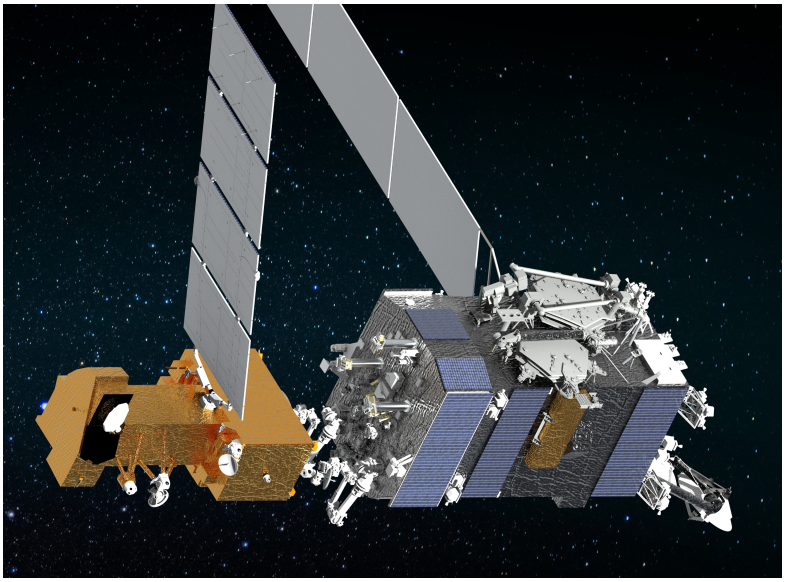

Figure 1.1. Concept of OSAM-1. Credit: NASA [15].

in GEO [17]. These Satlets were designed to incorporate essential satellite functionality with standard ports (for electronics, mass exchange, and data transfer) and to be reconfigurable and reassembled to accomplish different space missions.

Deutsche Orbitale Servicing Mission (DEOS) DEOS was a demonstrative mission carried out by the German Aerospace Centre (DLR). It involved two satellites, a chaser and a target, and the main goal was to find and evaluate procedures and techniques for rendezvous, capture and deorbiting of an uncontrollable satellite from its operational orbit [19].

Mission Extension Vehicle (MEV) The Mission Extension Vehicle programme (MEV-I and MEV-II) by Northrop Grumman/Orbital ATK are two ongoing commercial missions whose objective is to extend the life of existing GEO satellites that are low on fuel. They are designed to service multiple satellites from clients and carry fuel for a planned 15+ year service life [14].

On-Orbit Servicing, Assembly and Manufacturing (OSAM) The mission On-Orbit Servicing, Assembly and Manufacturing OSAM-1 will dock on an operational satellite and refuel it to extend its operational life [15]. The OSAM-1 spacecraft will also have an attached payload called Space Infrastructure Dexterous Robot (SPIDER). SPIDER will combine seven elements to create a functioning

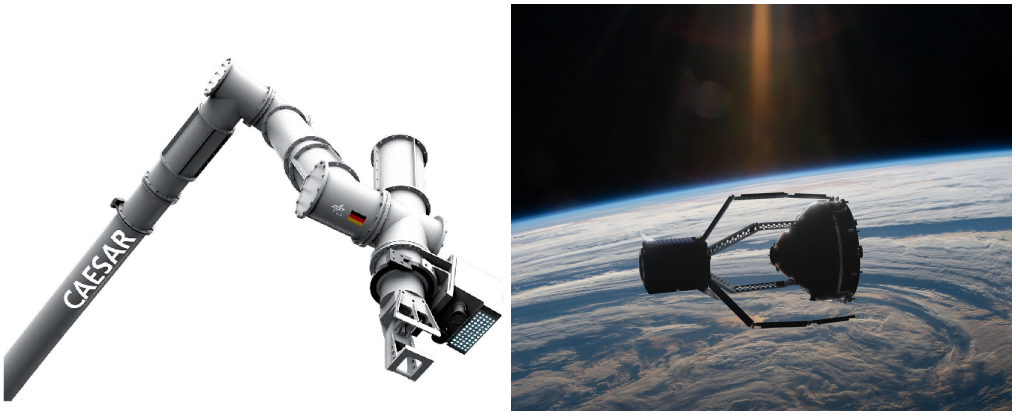

Figure 1.2. Concept of CAESAR at left and of Clearspace-1 at right. Courtesy of the Institute of Robotics and Mechatronics - DLR [8] and The European Space Agency [7].

3 meter antenna and will also produce 10-meter-long lightweight composite beams. The assembly and manufacturing element of the demonstration will verify the capability to construct large spacecraft structures in orbit. An artist's concept of OSAM-1 is represented in Fig. 1.1.

A second mission is planned and is expected to launch no earlier than 2024: OSAM-2. This is a technological demonstration of in-space additive manufacturing. The satellite will build two beams and deploy a surrogate solar array utilising robotic manipulation [16].

Compliant Assistance and Exploration SpAce Robot (CAESAR) German Aerospace Centre (DLR) is developing CAESAR (represented on the left in Fig. 1.2), a robotic arm designed for a variety of on-orbit services, for example, assembly, maintenance, repair, and debris removal in LEO or GEO [8], continuing to work on OOS that began with DEOS.

ClearSpace-1 The ClearSpace-1 ESA mission is planned to launch in 2026 and will rendezvous with, capture, and safely bring down a 112 kg defunct rocket part launched in 2013 for safe atmospheric reentry [7]. An artistic's representation is on the right in Fig. 1.2.

In space manufacturing and assembly (ISMA) European Space Agency (ESA) funded the project of the first metal 3D printing machine in space. Developed by Airbus, a technological demonstrator will launch in the near future to operate on the International Space Station, in order to validate the technology in microgravity but in protected environmental conditions. The ambition is that

in the future metal derived from recycled parts from decommissioned satellites will be used to build metal structures in situ [13].

1.2 Introduction to AUTOMA project

The AUtonomous Technologies for Orbital servicing and Modular Assembly (AUTOMA) is a project founded at the Department of Industrial Engineering at the University of Padova. The aim of the project is to carry on the development of the SMArt Capture Kit (SMACK) developed in [2]. The advancements regard the SMACK involvement in manipulation of objects, in order to perform OOS and IOA tasks.

The foreseen mission scenarios proposed by this project are two: the first application is related to autonomous IOA type of mission, the second is related to automatic structural assembly by means of drones or other small vehicles, both on Mars or other remote and risky areas on Earth.

1.2.1 Project objective

Regarding the first mission scenario, the objective of the project is to use SMACK to conduct system experiments such as:

1. Relative motion estimation of cooperative or non-cooperative small satellite mock-up floating on low-friction table reproducing the free falling motion of an orbiting satellite;
2. Robotic assembly of cooperative nano-satellite modules onto a vehicle that reproduces the orbital dynamics.

The first aims to test the technology for mission scenarios such as the inspection of cooperative and non-cooperative assets, and to verify the correctness of the relative pose estimation by the sensor suite.

The second (shown in Fig. 1.3) is intended to test the technology for an IOA mission, i.e. to enhance existing satellite capabilities, revive decommissioned assets, or dispose of debris. These are satisfied by attaching one or more servicing modules to the target system, which are called Elementary Assembly Units (EAUs).

This scenario involves several phases:

1. The robotic arm of the chaser vehicle is equipped with SMACK, which drives it to the EAU. The modular element is in a known location called *storage*;

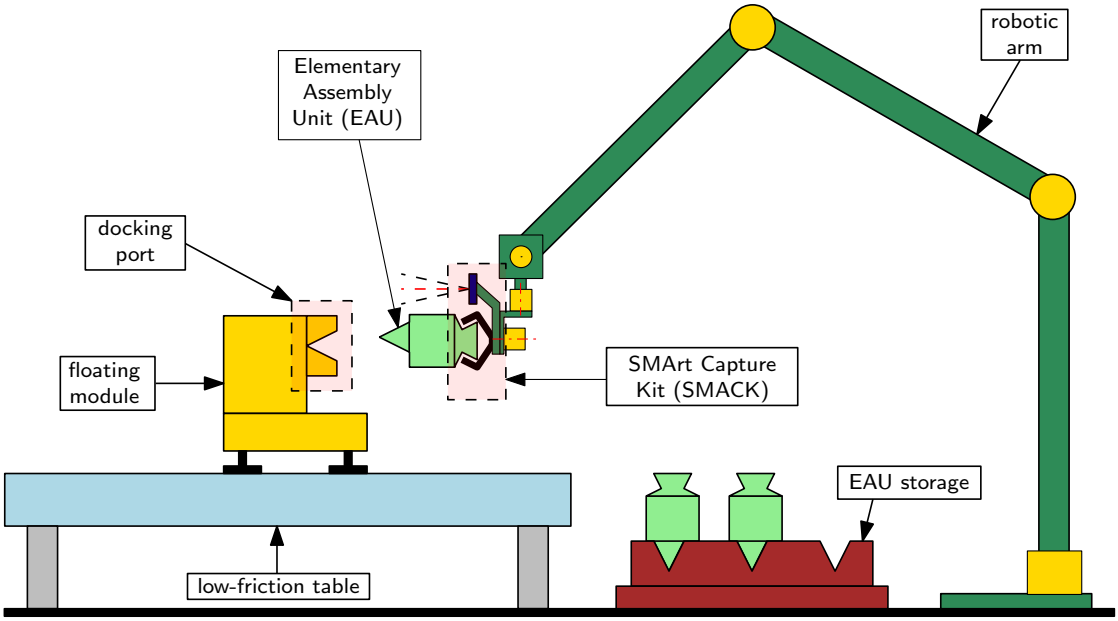

Figure 1.3. Schematic representation of AUTOMA project system experiment.

2. The sensor suit of SMACK is used to accurately estimate the location and pose of the EAU and allows SMACK to capture it;

3. SMACK drives the robotic arm to the target structure on which the EAU will be mounted;

4. The sensor suit of SMACK accurately estimates the location and pose of the docking port, which is located on the target structure. SMACK attaches the EAU to the target thanks to its docking mechanism. The assembly phase ends once the EAU is rigidly connected to the target structure.

1.3 Purpose of this work

The objective of this work is to conduct experiments for the AUTOMA project, in particular experiments on a suite of relative navigation sensors that provide accurate pose estimation, which enables the autonomous assembly of modular structures and is applicable to IOA scenarios.

The aim is to have a thorough understanding of the behaviour of the system and to understand how to improve it. At the same time, this work contributes to the promotion of the concepts of modularity and flexibility in the design of space systems and emphasises the innovative possibilities offered by the concepts of OOS and IOA.

The AUTOMA project activities foresee a first part of *sub-system design* of:

- Elementary Assembly Unit (EAU), its capture features and docking mechanisms, and the design of the electronic circuit to manage them. The docking mechanism is adapted from [1];
- SMACK upgrades (shown in Fig. 1.4), which are:
  - **Sensor package upgrade**: a ToF sensor has been added, going from three ToFs to four. The second upgrade is the design of a matrix sensor to measure the roll angle of the EAU;
  - **Mechanical upgrade**: the structure of SMACK is reviewed in order to reduce its mass, to accommodate the new sensors, and to accommodate linear actuators for the fingers instead of rotary servomotors. Also, the fingers and EAU capture interfaces are re-shaped; the capture interfaces present a concave slot to accommodate the fingers in order to establish a rigid connection with it.

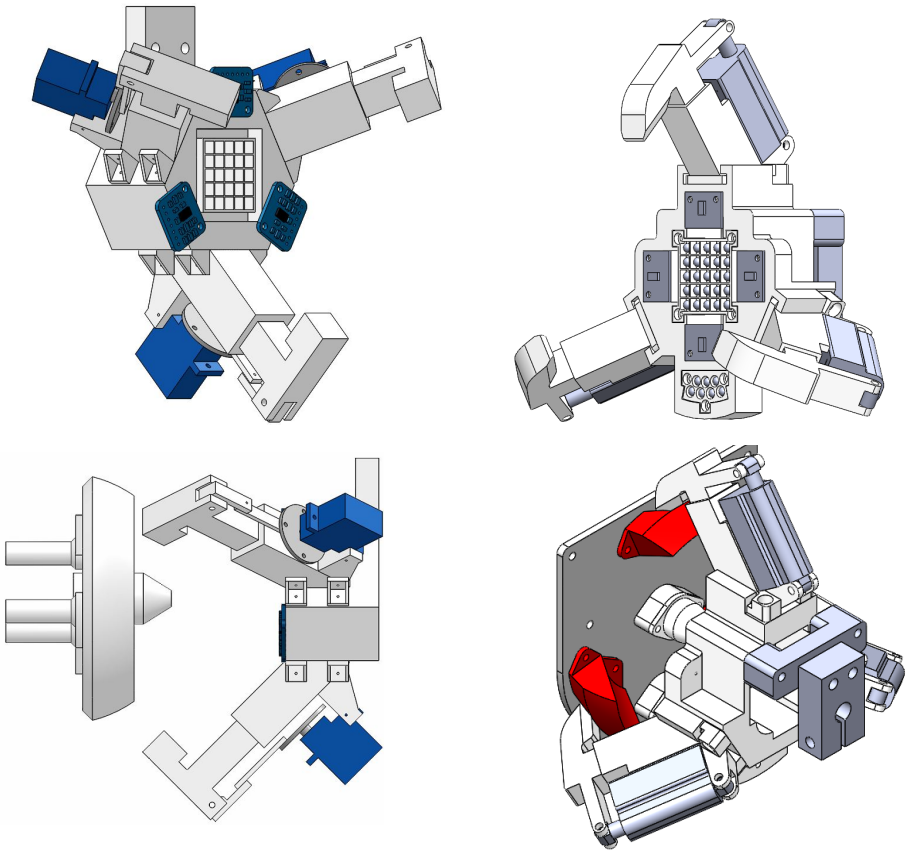

Figure 1.4. CAD model of SMACK prototype version on the left and of the upgraded version on the right (developed within the AUTOMA project).

The *experimental activities* are conducted in the second part. The solutions designed are tested to get a complete understanding of the behaviour of the system. The tests foreseen for the AUTOMA project are the following:

1. **Component level tests**: tests of all the components selected, in order to identify defects or bugs and to validate if performances are as expected;
2. **Sub-system level tests**: performed as a prelude to system testing. It is performed in the operating environment using the hardware and software of the installed subsystems. Subsystem testing must verify all functional requirements and verify its standalone performance;
3. **System level tests**: performed in the operational environment using all available hardware and software of the system previously installed and tested. These tests follow the logic of testing with an increasing level of complexity:
    - **Open-Loop test**: involves the integrated systems but no feedback loop is implemented at this stage. The aim is to validate system mechanisms;
    - **Closed-Loop tests**: a feedback loop is implemented on the sensor measurements so that the system acts autonomously. The mission scenario is divided into blocks of single tasks, and each one is tested. These leads to the overall system test where all tasks are performed consecutively.

Since the activities of subsystem design and component choice have already been carried out, this work focuses on the experimental activities, and in particular foresaw the following activities (summarised in Fig. 1.5):

1. Design of the EAU circuit;
2. Manufacturing and integration of hardware components inside the test setup;
3. Component-level tests: tests on finger actuation, test on EAU docking mechanism actuation, characterisation tests of SMACK sensor suite (ToF, in-plane matrix and roll matrix sensors);
4. Subsystem level tests: TOFs estimation algorithm test, SMACK capture and holding tests;
5. Open-loop system test: approach and capture without the feedback derived from sensor suite measurements. These tests are intended to validate overall system mechanisms;

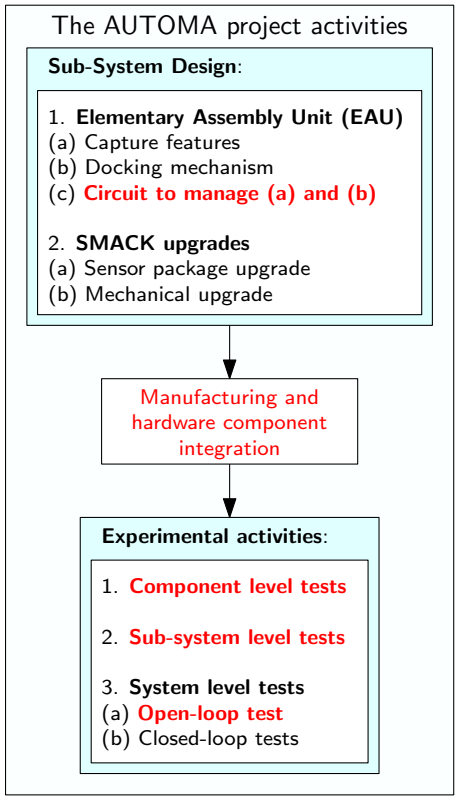

Figure 1.5. Summary of the activities foreseen by the AUTOMA project, with a focus on the activities carried out in the context of this work.

The organisation of the manuscript is as follows:

Chapter 2 is an overview of all aspects (mechanical, sensors, actuators and electronic) of SMACK and EAU;

Chapter 3 describes the Navigation Algorithm used to improve the pose estimation of SMACK sensors;

Chapter 4 illustrate and discusses the results of the subsystem level test performed on the SMACK sensor suit (which includes the Navigation Algorithm) and of open-loop system test;

Chapter 5 summarises the main results and provides future steps to complete the development of the AUTOMA project.

2

SMACK and EAU overview

This chapter describes the components of the SMArt Capture Kit (SMACK), of the Elementary Assembly Unit (EAU), and the related hardware.

2.1 SMArt Capture Kit (SMACK)

The peculiarity of SMACK is that it is an independent system from the robotic arm on which it is mounted: in the same fashion as in the prototype design [2], the computer of SMACK is independent from that of the space robot. The main parts of SMACK are shown in Fig. 2.1, and they are:

- A capture tool like a gripper consisting of three independently actuated fingers;
- A set of sensors whose measurements are fused together to estimate the pose of the target. The three sensors are four Time-of-Flight sensors and two custom phototransistor matrices. These are used to measure different Degrees of Freedom of the target;
- A computer that executes the algorithms needed to perform the capture. Specifically, the algorithms are the following:
  - A *navigation algorithm* that estimates the relative pose of the EAU with respect to the centre of SMACK, using measurements from all sensors (Chap. 3);
  - A *guidance algorithm* that creates the alignment and approach trajectory to the target;

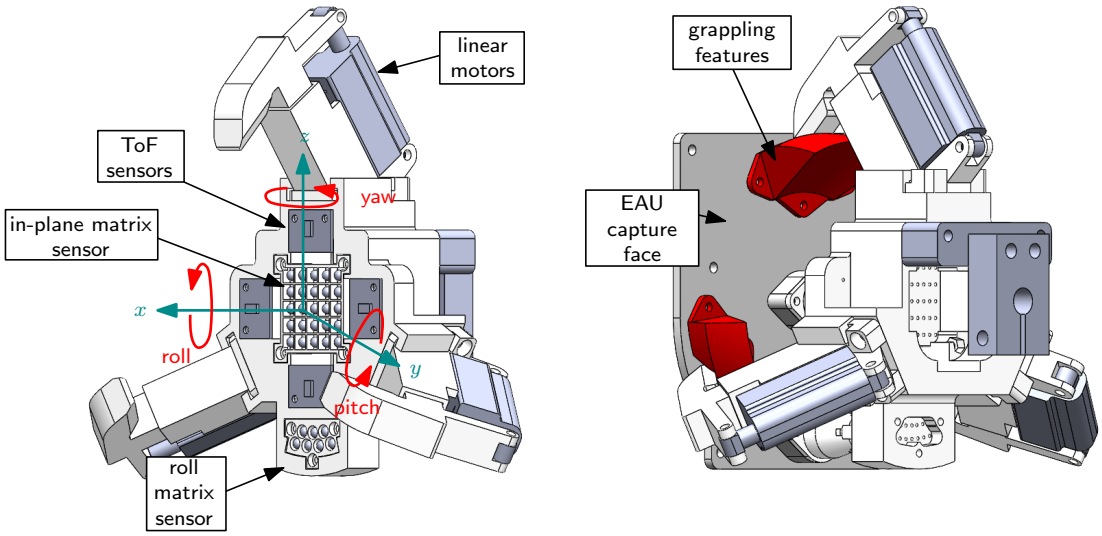

Figure 2.1. The gripper and grappling features. The sensors, the actuators and the reference system are highlighted.

– An algorithm that manages all sensors, controls the actuators, and implements a closure strategy for the fingers.

The first consequence of this design choice is that the gripper can be mounted on different types of robotic architectures; the second is that it is possible to distribute the control tasks. In particular, in Fig. 2.2, the conceptual diagram of how the capture tool interfaces with the robotic arm is represented. The gripper executes the Guidance and Navigation algorithms and executes the capture. The space robot, on the other hand, receives the pose information, computes the rotation and velocity of the joints, and executes the control of the robotic arm to bring the capture tool to the desired position for the capture.

2.1.1 The gripper

The gripper has three fingers individually driven by three linear motors (Actuonix PQ12-100-6-R). Linear motors are chosen because they allow fingers to be placed accurately (in extension and retraction).

The fingers are shaped to fit a concave slot in the three grappling interfaces on the EAU. Once aligned and in place, the gripper closes the fingers to capture and these tighten and adapt perfectly to the concavity (shown in Fig. 2.1).

The gripper manages to capture the target even if it is not perfectly aligned. The tolerated misalignments, as confirmed by experimental validation, are:

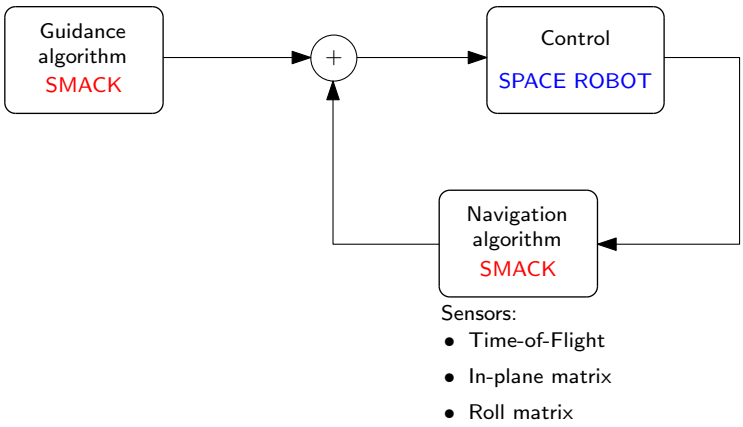

Figure 2.2. Conceptual architecture of the autonomous capture tool. SMACK provides to the computer of the robotic arm the desired pose in terms of way points, which are computed by its integrated computer.

- 12 mm along y axis;
- -10 mm to 15 mm along the z axis (due to its asymmetry);
- 9 deg in rotation around x axis;
- 5 deg in rotation around y axis;
- 10 deg in rotation around the z axis.

For further details on the tolerated misalignments, refer to Sect. 4.1.2, where the tests and results are described.

2.1.2 SMACK electronics

The computer of SMACK is a Raspberry Pi model 3B+, and manages all the electronic parts. To expand its capacities, it is connected to two expansion boards (shown in Fig. 2.3 and Fig. 2.4):

- *IoPi Plus AB Electronics* board: this expands the computer digital inputs with thirty-two additional inputs. It is used to read the twenty-five phototransistors of the positioning sensor and the seven phototransistors of the roll-angle sensor. It communicates with the Raspberry Pi via I2C communication.
- *Adafruit Servo Motor Pi Hat* board: this board produces the PWM signals for the three motors of the fingers. It communicates with the Raspberry Pi via I2C communication.

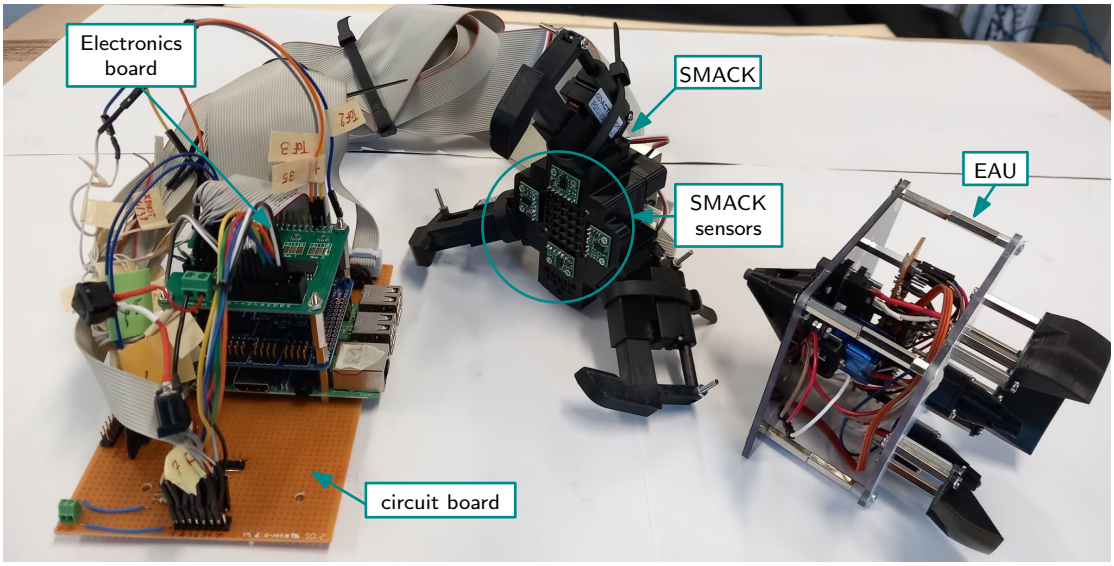

Figure 2.3. Overview of the main parts of SMACK and EAU.

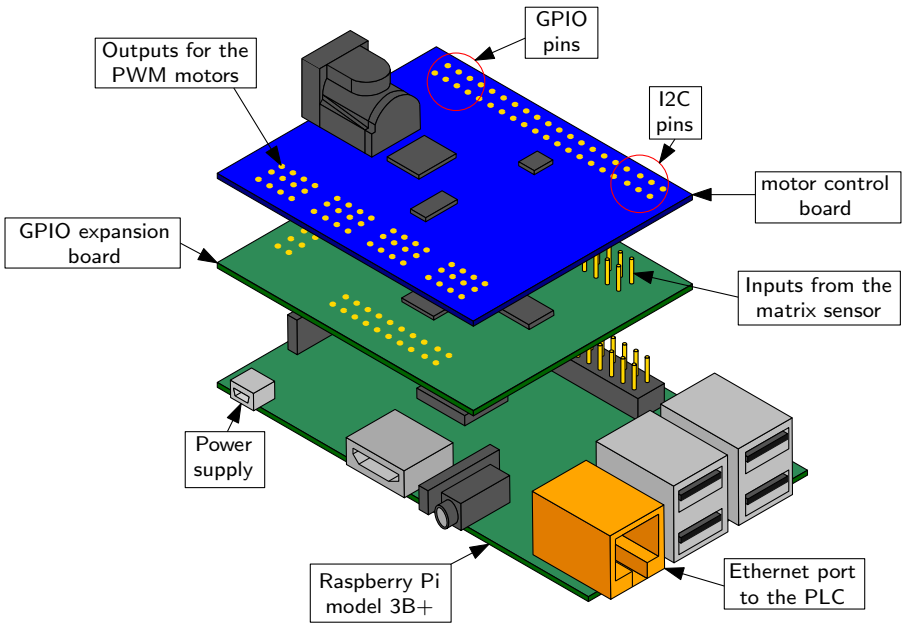

Figure 2.4. The main computer of the gripper (the Raspberry Pi model 3B+) with the two expansion boards to improve its capacity (GPIO expansion and Motor control).

In Fig. 2.5, the electronic circuit scheme is represented. This also shows the pinout schematics. Its main features are the following:

- All grounds and feeding (+5 V) lines are grouped;
- All the SDA and SCLK lines for the I2C communication of the Time-of-Flight sensors are grouped;
- It connects all the twenty-five pull-up resistors needed for the phototransistors of the in-plane matrix sensor;
- It connects all the seven pull-up resistors needed for the phototransistors of the roll matrix sensor.

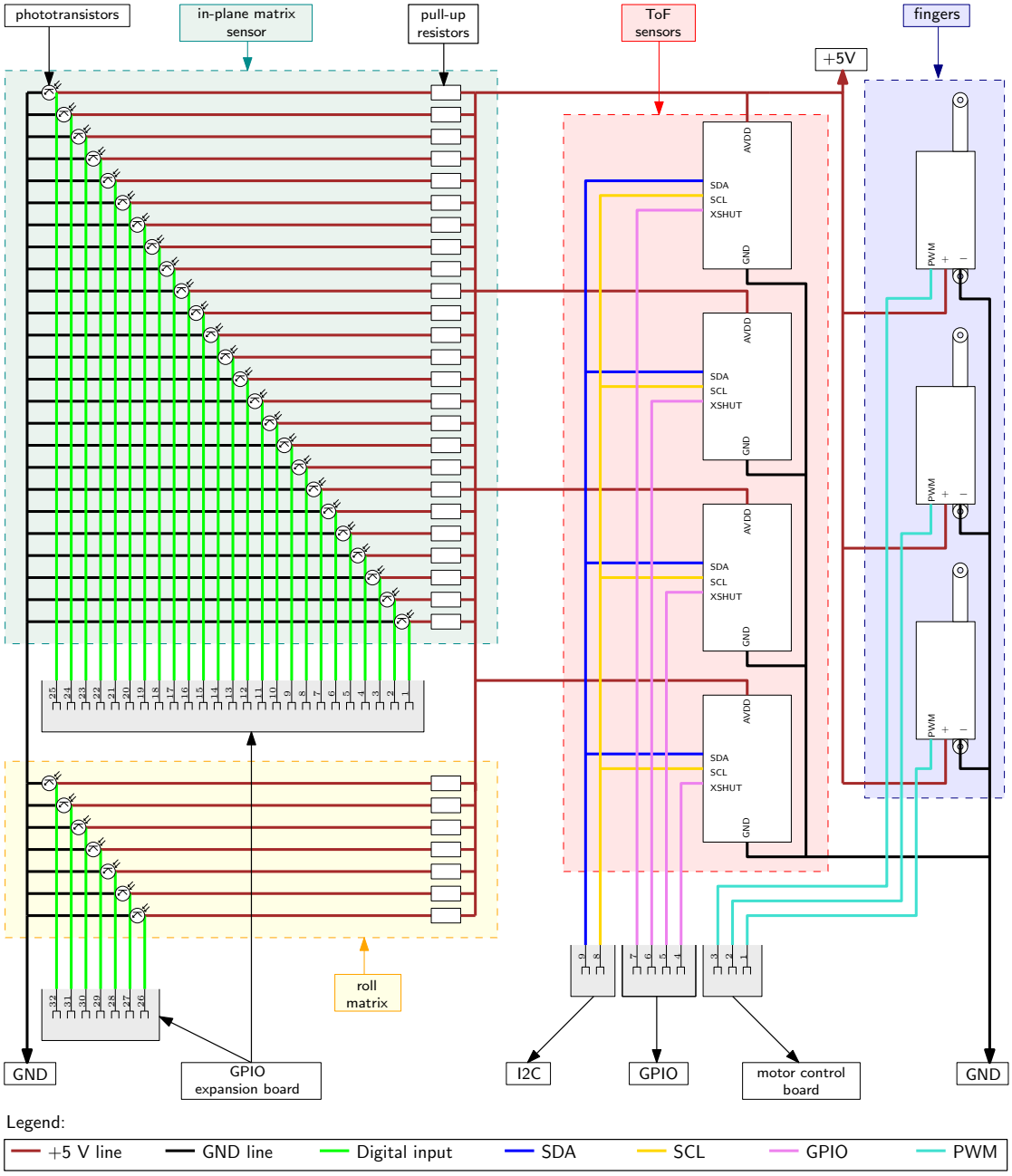

Figure 2.5. The custom electronic circuit that manages all sensors and their communication, feeding and ground lines.

2.1.3 Sensor package

The gripper is equipped with several sensors to measure the pose of the target, which are activated in different ways depending on the distance from the target. This section will describe in depth the various sensors, which are:

1. A Navigation Camera (RaspiCam V1.3), used to calculate the complete pose of the target in the approach phase and the assembly phase;
2. Four Time-of-Flight sensors, which measure the relative distance along the x direction and the pitch and yaw angles;
3. A custom matrix of twenty-five phototransistors arranged as a 5×5 matrix. Phototransistors detect infrared light and emit a certain current as output. The infra-red light source is located in the centre of the EAU capture face. This sensor measures the position in the $y - z$ plane and the distance along the x direction;
4. A custom matrix of seven phototransistors, following the same principle of the previously described matrix. This matrix reacts to an infra-red LED placed on the EAU capture face and measures the roll angle.

The operative ranges are shown in Fig. 2.6.

The navigation camera (NavCam) is used to reconstruct the pose of a pattern of fiducial LED markers mounted on the EAU capture face. This sensor has been fully characterised in [20]. The tests proved the ability of the NavCam to be used as a navigation sensor both for the first approach and for the assembly phases.

The NavCam estimates both position and attitude of the EAU up to a distance of 60 mm. This is because at a closer distance the camera is out of focus.

In an in-orbit mission scenario, it is assumed that up to that distance the gripper and the EAU are already aligned and have the same dynamics, thanks to the use of the NavCam. The three additional sensors listed above are used to carry out the remaining part of the approach manoeuvre and capture of the EAU.

The ultra-close approach phase is managed by the synergy between the ToF sensors (with an estimation algorithm) and the matrix sensors.

In Tab. 2.1, it is possible to see a summary of the main sensor measurement ranges, the measured quantity, and the relative operative phase. It is important to note that the sensor measurements overlap, so no phase of the approach is left without the pose measurement.

These operating ranges have been validated through tests that will be illustrated in Chap. 4.

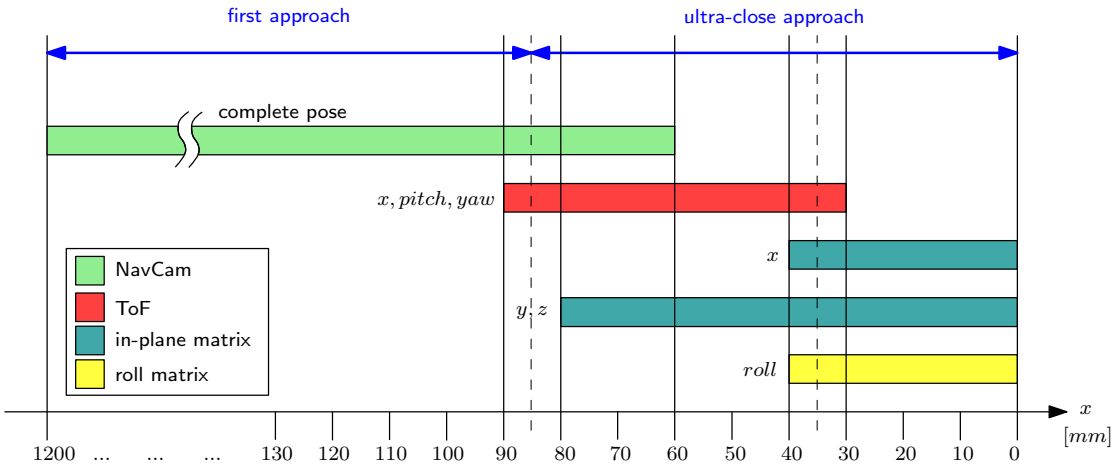

Figure 2.6. Summary diagram of the phases in relation to the sensors used and the quantity measured.

Phase	**Sensor**	**DoF measured**	**Range** [mm]
First approach Assembly	NavCam	complete pose	1200 ÷ 60
Ultra-close approach	ToF sensors	x, pitch, yaw	90 ÷ 30
	Matrix sensor	x	40 ÷ 0
	Matrix sensor	y, z	80 ÷ 0
	Roll sensor	roll	40 ÷ 0

Table 2.1. The operative ranges of all the sensors employed in SMACK in relation to the phase.

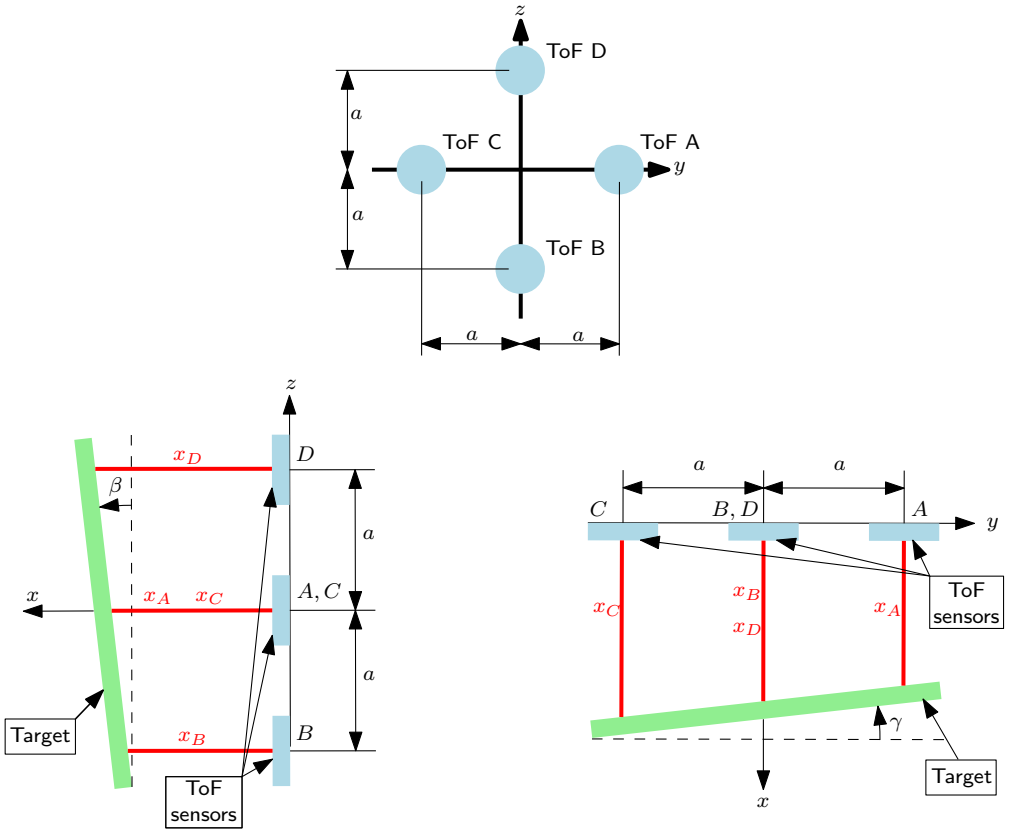

Figure 2.7. The position of the ToF sensors in the frontal face of SMACK. It is also represented that, if the target is tilted, sensors measures are different. β and γ are, respectively, the pitch and yaw angles.

Time-of-Flight sensors

The four Time-of-Flight sensors are VL6180 sensors by Pololu Electronics and are used for proximity distance and attitude measurements. They use time-of-flight measurements of infra-red pulses for ranging, allowing relative distance to be measured independently by the target reflectance. The measurement range of ToF sensors is theoretically from 100 mm to 0 mm. However, at a distance lower than 35 mm, the noise increases drastically and for this reason, in SMACK they are limited to > 35 mm. They communicate with the Raspberry Pi through I2C communication. The theoretical accuracy is 1 mm with an error of ±2 mm.

ToF sensors are arranged around the centre of the gripper as illustrated in Fig. 2.7. They are equally spaced with respect to the centre and at a distance a equal to 23.4 mm.

Thanks to the measurements of the four ToF sensors, it is also possible to compute the pitch and yaw angles (β and γ, respectively, in Fig. 2.7): in fact,

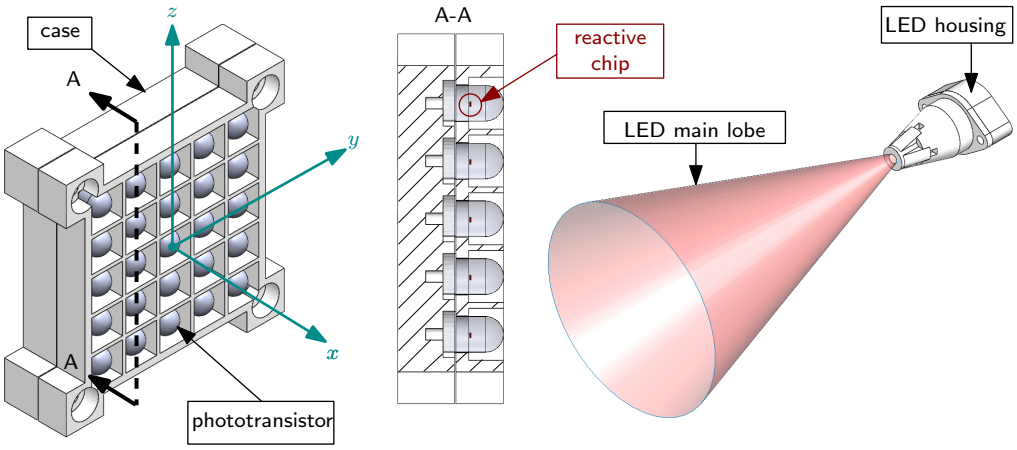

Figure 2.8. The in-plane matrix sensor with its two main parts: the matrix of twenty-five phototransistors and the infra-red LED.

when the target is rotated, the ToF sensors measure different distances and through these it is possible to calculate the $\tan\beta$ and $\tan\gamma$ as follows:

$$\tan\beta = \frac{x_D - x_B}{2a} \qquad \tan\gamma = \frac{x_C - x_A}{2a} \tag{2.1}$$

To improve the estimation of the pose of the ToF sensors, a Navigation Algorithm is used. This will be illustrated in Chap. 3, while in Sect. 4.2.2 the performed tests and the related results will be illustrated.

In-plane Matrix sensor

The matrix sensor is composed by two parts (as shown in Fig. 2.8):

- A 5×5 matrix of phototransistors whose centres are spaced by 5 mm each;
- An infra-red LED (L-7104F3C) mounted on the EAU capture face, whose conic beam operates as an optical beacon. The semi-viewing angle is about 17 deg.

Phototransistors are housed inside a body, which consists of two parts: the lower part where the phototransistors are housed; the upper part that holds the phototransistors tight and in place. The top piece, in particular, is made so that the reactive chip of the photransistor is clearly visible. In this way, the field of view of the phototransistor is not limited.

The operating principle is as follows: the LED cone activates a certain number and a certain pattern of phototransistors according to the distance in x between

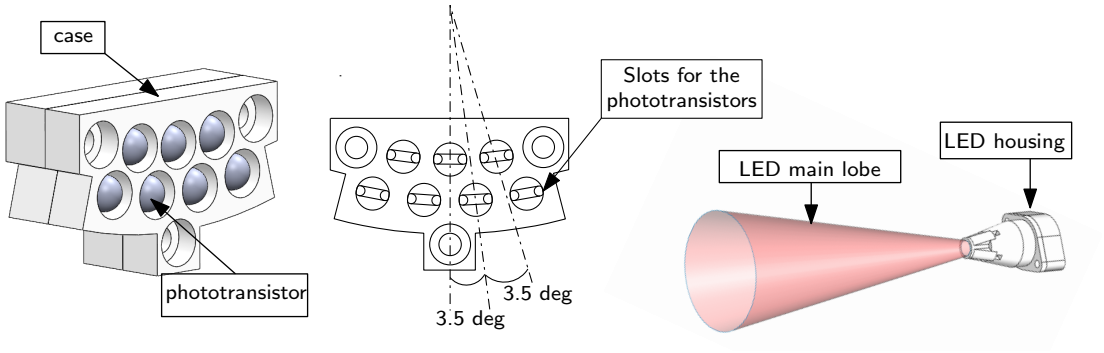

Figure 2.9. The roll matrix sensor with its two main parts: the matrix of seven phototransistors and the infra-red LED.

them and according to the angle of rotation. The active phototransistors pattern will be a square, a rectangle, or other type of pattern. Based on the dimension of the pattern, it is possible to reconstruct the position along the x, y, and z axes of the EAU.

The position along the y and z axes is computed as the distance of the centroid of the pattern of active phototransistors with respect to the centre of the sensor.

This sensor is also able to calculate the distance from the target along the x direction: this is performed by using a second-order polynomial equation as follows:

$$x = a_0 + a_1 \cdot N + a_2 \cdot N^2 \tag{2.2}$$

where N is the number of active phototransistors. The coefficients are experimentally found with the set of data in [3]. They are: $a_0 = -1.15$, $a_1 = 0.50$ and $a_2 = 0.07$.

The tests performed on the in-plane matrix sensor to assess its performance are illustrated in Sect. 4.2.3.

Roll Matrix sensor

Both the sensors described in the previous sections are not able to measure the relative roll angle. This is necessary as the EAU capture face is not axial-symmetric. The sensor is designed in a similar way to the matrix sensor, as illustrated in Fig. 2.9. Its two main parts are:

- A matrix of seven phototransistors, divided on two concentric arcs (three on the internal arc and four on the external arc alternately) and equally spaced by 3.5 deg;

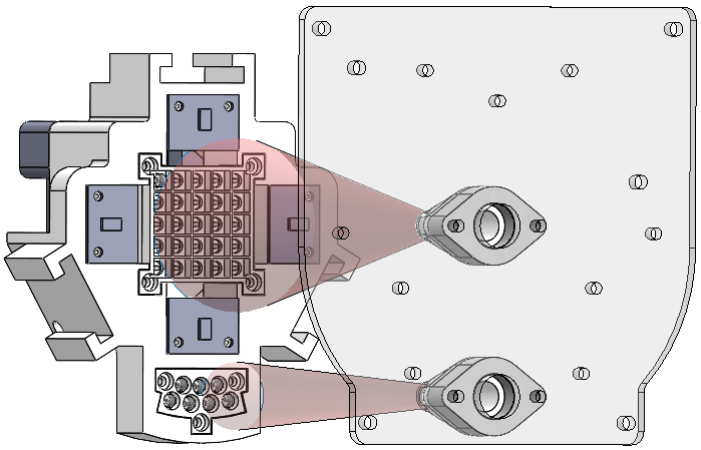

Figure 2.10. Caption

- An infra-red LED (SFH 4544) mounted on the EAU face, whose conic beam operates as an optical beacon. The semi-viewing angle is 10 deg.

The phototransistors are housed in a body in the same way as the in-plane matrix.

To measure the roll angle, the gripper must be centred with respect to the EAU. As represented in Fig. 2.10, this is due to the fact that if a misalignemnts in $y - z$ plane occurs, the roll matrix sensor provides an output different from zero.

The roll angle is measured by computing the angular distance of the centroid of the activated phototransistors with respect to the centre of the sensor.

The tests performed on the roll matrix sensor to assess its performances are illustrated in Sect. 4.2.4.

2.2 Elementary Assembly Unit (EAU)

The Elementary Assembly Unit (EAU) acts as a mock-up of an assembly module with basic functionality. The faces have dimensions of a square of side 100 mm, the same dimensions of a cube-sat. The elements that compose it are the following:

1. Three grappling interfaces used for the capture;
2. Two infra-red LEDs, which are used for the estimation of the target position (Fig. 2.11);

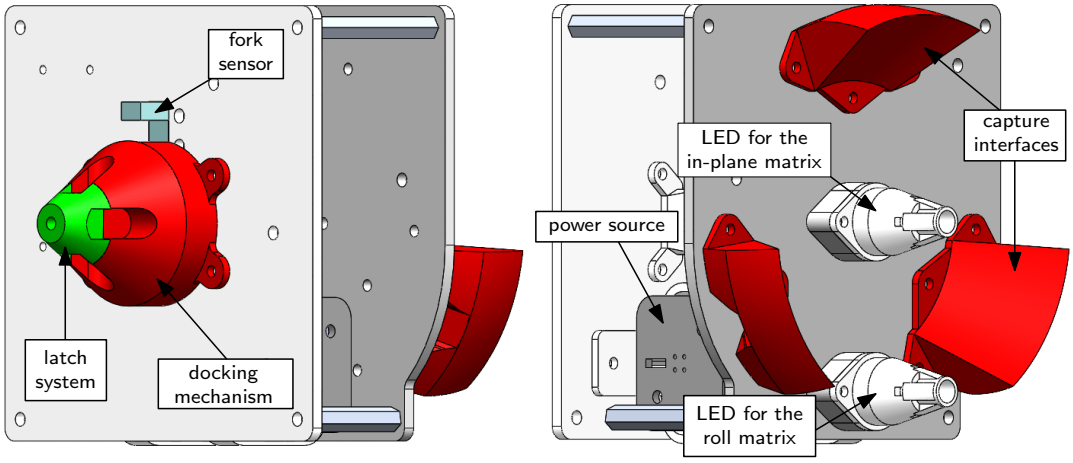

Figure 2.11. CAD model of the Elementary Assembly Unit (EAU) with its main components.

3. The docking mechanism, which is employed to mount the EAU on the target structure;

4. Micro-controller (Arduino micro), its circuit, and power supply to manage the docking mechanism and to activate the infra-red LEDs.

2.2.1 Docking mechanism

In Fig. 2.12 it is possible to see the docking mechanism and the docking port (the drogue). This is a miniaturized docking system specifically designed for cube-sat platforms (fully described and validated in [1]), and works as follows:

- When the EAU and the docking port are aligned, the probe freely enters the drogue. The tip can rotate and is connected to the motor with a shaft;
- The rim of the drogue activates the fork sensor. At that point, the logic of the circuit activates the motor which rotates the tip of the probe by 45 deg;
- When rotating, the tip is blocked by the rigid overhangs present in the drogue, making the connection between the two parts rigid.

2.2.2 EAU electronics

The EAU circuit is managed by an Arduino Micro, and its schematic representation is visible in Fig. 2.13. This is a microcontroller board based on the

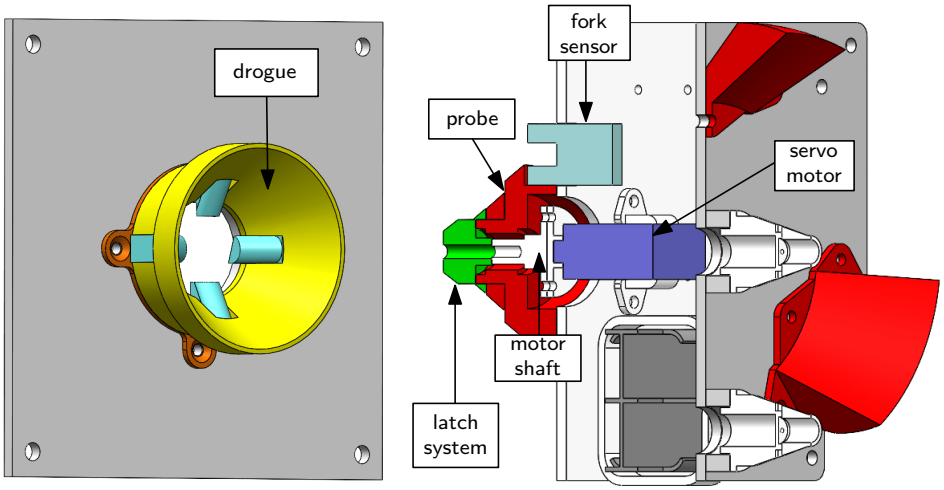

Figure 2.12. CAD model of docking mechanism with its main part and of the docking port (the drogue).

ATmega32U4. It has twenty digital input/output pins (of which seven can be used as PWM outputs and twelve as analog inputs/outputs).

The circuit has been realized taking into account two factors. The first is the limited internal space, which leads to the desire to use the same power supply for all circuit elements. The second major aspect is that the servo motor introduces noise on the power line.

This fact is of particular importance, as the Arduino Micro needs a stable supply voltage for its proper functioning.

The power supply values required for the various elements are:

- Arduino micro: $7 \div 12$ V;
- FITEC FS90 Micro Servo: 6 V;
- OMRON Photomicrosensor (EE-SX673): $5 \div 24$ V.

This leads to the selection of the optimal voltage value at 8 V so that all users receive the correct voltage. To stabilise the power line, various solutions have been considered:

1. To use a low-pass filter (Fig. 2.14) to cut the signal that disturbs the power line. This signal follows the trend of the PWM signal of the digital output pin of the Arduino. The disturbing signal has an amplitude of 49 Hz and a period of 20 ms. The filter consists of a resistor and a capacitor with resistance and capacitance equal to $R = 1\,\text{M}\Omega$ and $C = 0.1\,\mu\text{F}$. The cutting frequency is given by $f_c = \frac{1}{2\pi RC} = 1.59\,\text{Hz}$. Unfortunately, if a power

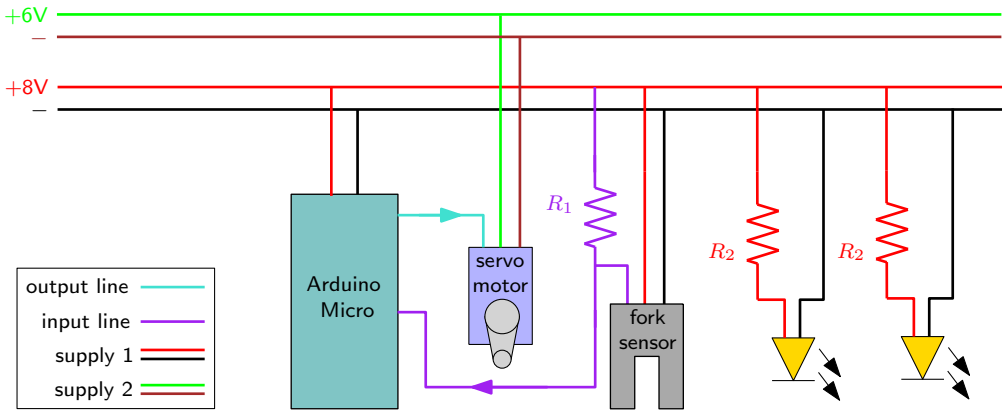

Figure 2.13. Schematic representation of EAU circuit.

supply of 8 V is used, the RC filter introduces a high voltage drop which does not allow the sensors and actuators to be correctly powered, even if this method stabilises the power line;

2. To use two different power supplies: one for the motor and one for the other devices. In this way two power supplies would be used at 6 V and 8 V respectively, with the drawback of the increase in weight and the reduction of EAU internal space;

3. Introducing a voltage regulator: this element, combined with the use of two capacitors as shown in Fig. 2.14 is capable of stabilising the power line, using only one power supply for the whole circuit. However, for an output voltage of 8 V an input voltage of 14 V is required. Therefore, this way of proceeding proves to be the most space-consuming.

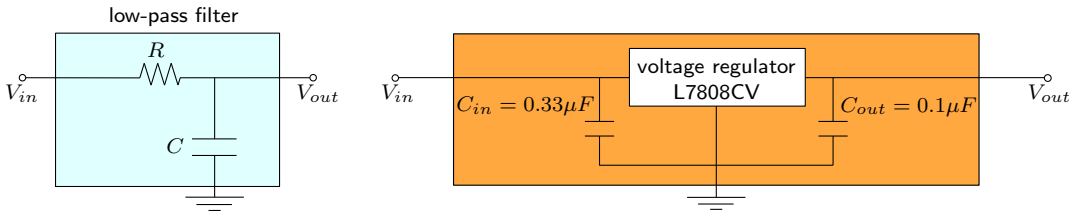

Figure 2.14. Low-pass filter and voltage regulator scheme.

Consequently, solution at point 2, with two separate power supplies is the one to prefer. In this way, no other elements are added to the circuit, and it is possible to better distribute the weight of the batteries in the internal space of the EAU.

Having now established the operating voltage value at 8 V, it is necessary to use an adequate resistor to protect the LEDs. This resistance value is found

through the maximum allowed current value of the individual LEDs. For both of them, this value is equal to $I_{max} = 100\,\text{mA}$. The required resistance value is therefore $R_2 = V_{batt}/I_{max} = 80\,\Omega$.

The fork sensor is connected to a pull-up resistor of $R_1 = 10\,\text{k}\Omega$ in order to have the correct voltage required by the input of the Arduino Micro.

3

Navigation Algorithm

The navigation algorithm is composed of two parts: the sensor management of the three SMACK sensors and the relative pose estimation.

The sensor management part is based on a logic that determines which sensor to use to estimate the EAU pose. The algorithm chooses the sensor based on the operative distance of each sensor, as explained in Chap. 2 in Sect. 2.1.3. These ranges are found through tests that will be illustrated in Chap. 4.

The estimation of the target pose provided by the ToF sensors is improved with the use of the Kalman filter. This is an iterative algorithm that predicts the state of the system, which is then updated using the sensors measurements.

In this chapter, the Kalman filter algorithm is described and a theoretical introduction to the state-space representation of dynamic systems and the state observer is given [12].

3.1 Theoretical introduction

3.1.1 State-space representation of Dynamic Systems

A multiple-input multiple-output dynamic system is described by differential equations like:

$$\dot{\mathbf{x}} = \frac{d\mathbf{x}}{dt} = f(\mathbf{x}, \mathbf{u}, t)$$

In a state-space model, three types of quantities are involved:

- m scalar input $u_1, u_2, \ldots, u_m$ that can be grouped into a vector called *input vector*;

- p scalar output $y_1, y_2, \ldots, y_p$ that can be grouped into a vector called *output vector*;
- n scalar state quantities $x_1, x_2, \ldots, x_n$ that can be grouped into a vector called *state vector*.

$$\mathbf{u}(t) = \begin{bmatrix} u_1 \\ u_2 \\ \vdots \\ u_m \end{bmatrix} \qquad \mathbf{y}(t) = \begin{bmatrix} y_1 \\ y_2 \\ \vdots \\ y_p \end{bmatrix} \qquad \mathbf{x}(t) = \begin{bmatrix} x_1 \\ x_2 \\ \vdots \\ x_n \end{bmatrix}$$

If the model is linear, the differential dynamic equations can be written in vector notation as follows:

$$\dot{\mathbf{x}}(t) = A \cdot \mathbf{x}(t) + B \cdot \mathbf{u}(t) \tag{3.1}$$

where the A and B matrices are given by:

$$A = \begin{bmatrix} a_{1,1} & a_{1,2} & \cdots & a_{1,k} \\ a_{2,1} & a_{2,2} & \cdots & a_{2,k} \\ \cdots & \cdots & \cdots & \cdots \\ a_{k,1} & a_{k,2} & \cdots & a_{k,k} \end{bmatrix} \quad B = \begin{bmatrix} b_{1,1} & b_{1,2} & \cdots & b_{1,l} \\ b_{2,1} & b_{2,2} & \cdots & b_{2,l} \\ \cdots & \cdots & \cdots & \cdots \\ a_{l,1} & a_{l,2} & \cdots & a_{l,l} \end{bmatrix} \tag{3.2}$$

The matrix A is the *state* or *system matrix* and B is the *input matrix*; A is always a square matrix ($n \times n$) while the size of B ($n \times m$) depends on the number of inputs to the system. For example, if there is only one entry to the system, B will be a column vector. The two matrices A and B are fundamental for state-space control.

The *output vector* $\mathbf{y}$ is the vector of the measured quantities. In general, it might be different from the the state vector and a linear combination of the state and the input:

$$\mathbf{y}(t) = C \cdot \mathbf{x}(t) + D \cdot \mathbf{u}(t) \tag{3.3}$$

where C is the *output matrix* ($p \times n$) and D ($p \times m$) is the *feedthrough*. If C is not the identity matrix, the sensors are measuring some combination of the state variables. Without loss of generality, it is possible to consider $D = 0$ (the case of a strictly proper system). This means that the inputs have no influence on the measurements.

In the general formulation, all matrices are allowed to be time-variant (i.e. their elements can depend on time); however, in the common cases, the matrices

are time-invariant and, therefore, constant.

The time variable t can be continuous or discrete. In the latter case, the time variable k is usually used instead of t. When digital controllers such as Arduino or Raspberry Pi are used, the state is updated with a certain frequency, so the discrete time variable k is related to the sampling period (the inverse of the sampling frequency). Therefore, the general continuous-time and discrete-time systems (named Σ) are the following:

$$\Sigma \quad \rightarrow \quad \begin{cases} \dot{\mathbf{x}}(t) = A \cdot \mathbf{x}(t) + B \cdot \mathbf{u}(t) \\ \mathbf{y}(t) = C \cdot \mathbf{x}(t) + D \cdot \mathbf{u}(t) \end{cases} \qquad \begin{cases} \mathbf{x}(k+1) = A \cdot \mathbf{x}(k) + B \cdot \mathbf{u}(k) \\ \mathbf{y}(k) = C \cdot \mathbf{x}(k) + D \cdot \mathbf{u}(k) \end{cases} \tag{3.4}$$

3.1.2 State observer

The state observer is a method to estimate variables of the state vector $\mathbf{x}$ that are not directly measured by sensors. For example, it is possible to estimate the velocity using only distance sensors (without using the discrete derivatives).

For the observability it is necessary that all the states are observable, i.e. the pair of matrices (A, C) is observable. The observability matrix O is calculated as:

$$O = \begin{bmatrix} C^T & A^T C^T & (A^T)^2 C^T & \cdots & (A^T)^{n-1} C^T \end{bmatrix} \tag{3.5}$$

The pair (A, C) is observable if $\text{rank}(O) \geq n$. If instead $\text{rank}(O) < n$, only some states are observable and we cannot obtain information for $q = n - \text{rank}(O)$ states. As a result, more sensors are needed to estimate the entire state vector. In general, it is necessary to have a measurement for each state variable that is linearly independent.

The observed state (named $\tilde{\Sigma}$) has equations of the type:

$$\tilde{\Sigma} \quad \rightarrow \quad \begin{cases} \tilde{\mathbf{x}}(k+1) = A \cdot \tilde{\mathbf{x}}(k) + L[\mathbf{y}(k) - \tilde{\mathbf{y}}(k)] + B \cdot \mathbf{u}(k) \\ \tilde{\mathbf{y}} = C \cdot \tilde{\mathbf{x}}(k) \\ e(k) = \mathbf{y}(k) - \tilde{\mathbf{y}}(k) \end{cases} \tag{3.6}$$

where $\tilde{\mathbf{x}}$ is the estimated state vector. L is the observer matrix and e is the error between the observed and the real state. A block diagram representation is visible in Fig. 3.1. The observer matrix L is designed to make the difference between the true output and the estimated output tend to zero with the desired rate.

The observation matrix L is chosen so that:

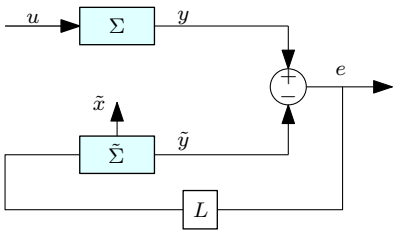

Figure 3.1. State observer block diagram.

- The $A - LC$ matrix has eigenvalues such that the system is stable
- The estimation error converges to zero faster than the control actions on the system.

There is the possibility to optimize the process, and the optimum observer is known as the Kalman-Bucy filter.

3.1.3 Kalman filter: optimum observer

The Kalman filter is a linear quadratic state estimator and provides the observation of the state with the lowest possible variance. The filter estimates the state based on both the evolution of the state and the measurements. The algorithm estimates the state by giving a greater weight to the model than to the measurements and vice versa. The choice is made based on the knowledge of the dynamic model and the noises of the measurements.

The filter considers that the dynamics of the state and the measurements are affected by a white Gaussian noise with zero mean v and w:

$$\begin{cases} \mathbf{x}(k+1) = A \cdot \mathbf{x}(k) + B \cdot \mathbf{u}(k) + v \\ \mathbf{y}(k) = C \cdot \mathbf{x}(k) + w \end{cases} \tag{3.7}$$

The noises are characterised by a covariance matrix that describes the uncertainty of the error and how it affects the state variables. These two covariance matrices are indicated with Q and R for v and w, respectively. These matrices can also be seen as weights for the system dynamics and measurement model:

- $Q < R$: the filter weights more the dynamic of the measurements than the dynamics of the model;
- $Q > R$: the filter weights more the dynamic of the model than the dynamics of the measurements.

The optimal observation matrix L is calculated iteratively until it assumes a constant value. The filter consists of six equations divided into two groups, three for prediction and three for update. The Kalman filter iterative algorithm is represented in Fig. 3.2.

Prediction The first three equations of the Kalman filter require: (1) the three matrices A, B C coming from the equations of dynamics of the system and the covariance matrices of the noises Q and R, (2) an initial estimation of the state vector $\mathbf{x}_{post}$ and (3) an initial estimation of the covariance matrix of the estimated state P_{post}.

It then makes a prediction of the state vector and of the covariance matrix at the next time step only on the basis of equations of dynamics of the system, named $\mathbf{x}_{pre}$ and P_{pre} respectively. Based on this estimation, it calculates the optimum observation matrix L. The three prediction equations are:

$$\begin{cases} \mathbf{x}_{pre} = A \cdot \mathbf{x}_{post} + B \cdot \mathbf{u} \\ P_{pre} = A \cdot P_{post} \cdot A^T + Q \\ L = P_{pre} \cdot C^T \cdot \left[C \cdot P_{pre} \cdot C^T + R \right]^{-1} \end{cases} \tag{3.8}$$

Update A measurement is made with the sensors to calculate the error between the real measurement and the prediction. This is then used to correct and update the prediction of the state vector. The covariance matrix is also corrected thanks to the error. The three update equations are:

$$\begin{cases} \mathbf{err}_y = \mathbf{y} - C \cdot \mathbf{x}_{pre} \\ \mathbf{x}_{post} = \mathbf{x}_{pre} + L \cdot \mathbf{err}_y \\ P_{post} = P_{pre} - L \cdot C \cdot P_{pre} \end{cases} \tag{3.9}$$

Once converged, the observation matrix L and the covariance matrix P remain constant and are no longer updated.

3.2 Model-based relative pose estimation

Regarding this work, a Kalman filter algorithm is implemented to improve the measurement of the pose of the EAU performed with the ToF sensors, in the same way as in [2]. As explained in Sect. 3.1.3, Kalman filter is an optimum state

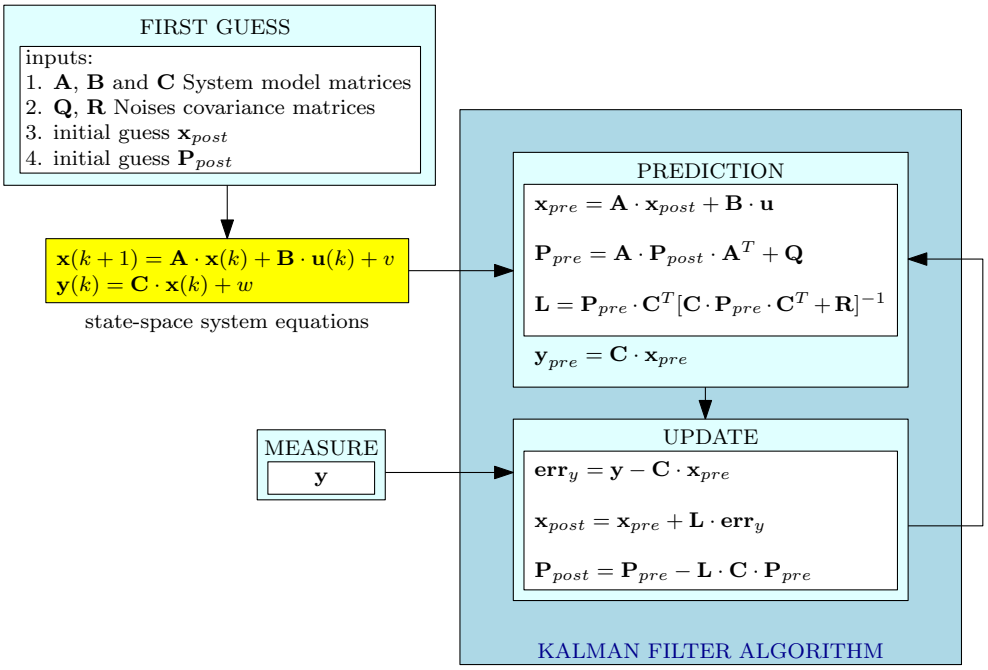

Figure 3.2. Kalman filter loop.

observer: This means that, due to the measurement of the distance sensors, it is possible to estimate other variables that are not directly measurable, in this case the approaching velocity. In addition, this estimate will have as little variance as possible.

The linear model equations are the following:

$$\begin{cases} \mathbf{x}(k+1) = A \cdot \mathbf{x}(k) + v \\ \mathbf{y}(k) = C \cdot \mathbf{x}(k) + w \end{cases}$$

with:

- $\mathbf{x} = \left[\overline{x}, \dot{\overline{x}}, \tan(\beta), \dot{\tan}(\beta), \tan(\gamma), \dot{\tan}(\gamma)\right]^T$ the state vector;
- $\mathbf{y} = \left[x_A, x_B, x_C, x_D\right]^T$ the measurements vector.

Referring to Fig. 3.3, the quantities taken into consideration are:

- $\overline{x}$: the average position of the EAU along the x axis with respect to the centre of the ToF sensors;
- $\tan\beta$ and $\tan\gamma$: the relative yaw and pitch angle;
- x_i, with $i = A, \ldots, D$: the measurements of the four ToF sensors;

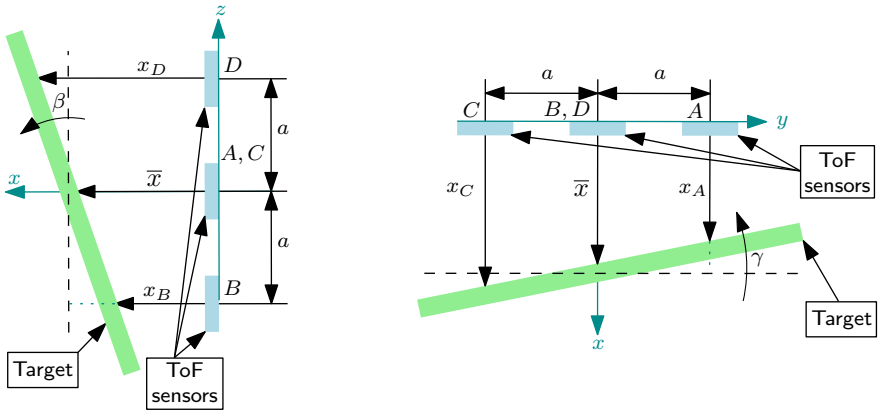

Figure 3.3. ToF sensors configuration.

- a: the distance between the ToF sensor and the centre of SMACK;
- Δt: the sampling time of the ToF sensors;
- v, w: the noises that affect the dynamic model and the measurements, respectively.

Dynamic model equation Considering a uniform motion (constant velocity), the discrete equations describing the behaviour of the system are the following:

$$\text{x distance} \rightarrow \begin{cases} \overline{x}_{k+1} = \overline{x}_k + \dot{\overline{x}}_k \cdot \Delta t \\ \dot{\overline{x}}_{k+1} = \dot{\overline{x}}_k \end{cases}$$

$$\text{pitch angle} \rightarrow \begin{cases} \tan\beta|_{k+1} = \tan\beta|_k + \dot{\tan}\beta|_k \cdot \Delta t \\ \dot{\tan}\beta|_{k+1} = \dot{\tan}\beta|_k \end{cases}$$

$$\text{yaw angle} \rightarrow \begin{cases} \tan\gamma|_{k+1} = \tan\gamma|_k + \dot{\tan}\gamma|_k \cdot \Delta t \\ \dot{\tan}\gamma|_{k+1} = \dot{\tan}\gamma|_k \end{cases}$$

By grouping the equations in a matrix form, the dynamic equation of the system becomes:

$$\begin{bmatrix} \overline{x} \\ \dot{\overline{x}} \\ \tan\beta \\ \dot{\tan}\beta \\ \tan\gamma \\ \dot{\tan}\gamma \end{bmatrix} (k+1) = \begin{bmatrix} 1 & \Delta t & 0 & 0 & 0 & 0 \\ 0 & 1 & 0 & 0 & 0 & 0 \\ 0 & 0 & 1 & \Delta t & 0 & 0 \\ 0 & 0 & 0 & 1 & 0 & 0 \\ 0 & 0 & 0 & 0 & 1 & \Delta t \\ 0 & 0 & 0 & 0 & 0 & 1 \end{bmatrix} \cdot \begin{bmatrix} \overline{x} \\ \dot{\overline{x}} \\ \tan\beta \\ \dot{\tan}\beta \\ \tan\gamma \\ \dot{\tan}\gamma \end{bmatrix} (k) + v \tag{3.10}$$

The system is linear since the tangent of the angle is used. The model represents a constant-velocity dynamic between SMACK and the EAU since the estimation is performed when SMACK and the EAU are not moving with respect to each other.

Measurement model equation Concerning the measurements of the ToF sensors, they measure a distance along x which can be related to attitude as follows:

- ToF B and D measure the pitch angle:

$$\begin{cases} x_B|_k = \overline{x}_k + a \cdot \tan\beta|_k \\ x_D|_k = \overline{x}_k - a \cdot \tan\beta|_k \end{cases}$$

- ToF A and C measure the yaw angle:

$$\begin{cases} x_A|_k = \overline{x}_k - a \cdot \tan\gamma|_k \\ x_D|_k = \overline{x}_k + a \cdot \tan\gamma|_k \end{cases}$$

The measurement equation of the Kalman filter model in matrix form becomes:

$$\begin{bmatrix} x_A \\ x_B \\ x_C \\ x_D \end{bmatrix}(k) = \begin{bmatrix} 1 & 0 & -a & 0 & 0 & 0 \\ 1 & 0 & 0 & 0 & a & 0 \\ 1 & 0 & a & 0 & 0 & 0 \\ 1 & 0 & 0 & 0 & -a & 0 \end{bmatrix} \cdot \begin{bmatrix} \overline{x} \\ \dot{\overline{x}} \\ \tan\beta \\ \dot{\tan}\beta \\ \tan\gamma \\ \dot{\tan}\gamma \end{bmatrix}(k) + w \tag{3.11}$$

It is possible to verify that the matrix O constructed using the pair (A, C) (Eq. 3.5) has $\text{rank}(O) \geq n$, with $n = 6$ the dimension of the state vector. Hence, the full state is observable, and the Kalman filter can be applied to estimate the velocity as well.

Initialisation Covariance matrices Q and R are symmetric matrices where the elements on the diagonal (${\sigma_{ii}}^2$) represent the variance (that is, by how much a variable deviates quadratically from the arithmetic mean), while the elements off the diagonal (${\sigma_{ij}}^2$) represent the covariance (describes how the change of one variable affects the other). The sign of the covariance shows the trend in the linear relationship between the variables: if the covariance is positive, it means that as one variable increases, the other also increases, while if the covariance

is negative, the opposite occurs. As one increases, the other decreases. If the covariance is zero, then the two variables are statistically independent.

The two covariance matrices Q and R are initialised with zero covariance for simplicity as follows:

$$Q = \begin{bmatrix} {\sigma_{Q_1}}^2 & 0 & 0 & 0 & 0 & 0 \\ 0 & {\sigma_{Q_2}}^2 & 0 & 0 & 0 & 0 \\ 0 & 0 & {\sigma_{Q_3}}^2 & 0 & 0 & 0 \\ 0 & 0 & 0 & {\sigma_{Q_3}}^2 & 0 & 0 \\ 0 & 0 & 0 & 0 & {\sigma_{Q_3}}^2 & 0 \\ 0 & 0 & 0 & 0 & 0 & {\sigma_{Q_3}}^2 \end{bmatrix} \rightarrow v \tag{3.12}$$

$$R = \begin{bmatrix} {\sigma_R}^2 & 0 & 0 & 0 \\ 0 & {\sigma_R}^2 & 0 & 0 \\ 0 & 0 & {\sigma_R}^2 & 0 \\ 0 & 0 & 0 & {\sigma_R}^2 \end{bmatrix} \rightarrow w \tag{3.13}$$

and the variance values are chosen as follows:

$$\begin{aligned} \sigma_{Q_1} = 1 \quad &\rightarrow \quad \overline{x}, \dot{\overline{x}} \\ \sigma_{Q_2} = 1 \quad &\rightarrow \quad \tan\beta, \tan\gamma \\ \sigma_{Q_3} = 0.02 \quad &\rightarrow \quad \dot{\tan}\beta, \dot{\tan}\gamma \\ \sigma_R = 1 \quad &\rightarrow \quad x_1, x_2, x_3, x_4 \end{aligned}$$

The value of σ_R represents the errors of the ToF sensors, while σ_Q have been chosen with a trade-off between the rate of convergence and the estimation performance.

The initialisation of $\mathbf{x}_{post}$ is carried out by physically measuring the distance of the ToF sensors from the EAU capture face with a measuring instrument.

Initialisation of $\mathbf{P}_{post}$ is set as an identity matrix 4×4.

From the tests it can be seen that the Kalman filter improves the estimation of EAU position and attitude compared to the use of ToF alone. For further details, see Chap. 4 in Sect. 4.2.2.

4

Test campaign

The main purpose of this work is to perform tests (at the component, subsystem, and system level) on SMACK and the EAU. The main tests are on the SMACK sensor suite to evaluate its static and dynamic performances. These sensors have the purpose to measure the pose and attitude of the target during the Ultra Close-Proximity Operations of the capture manoeuvre.

This chapter will describe the procedure and the results of each performed test.

4.1 Mechanical tests

4.1.1 SMACK capture and holding tests

The purpose of this test is to evaluate the capture, the actuation of all three motors, and their holding capacity. To do so, various weights in different configurations have been taken into account.

The clamping hold was tested both at the maximum expected load during EAU handling (approximately 0.4 kg) and by increasing the resistant weight to test its limits. The tested loads are visible in Tab. 4.1.

The performed tests are described below and listed by their ID:

1. EAU capture face is horizontal, all the gripper fingers are closed around the interfaces;

2. EAU capture face is vertical, all the gripper fingers are closed around the interfaces;

3. EAU capture face is horizontal, only two gripper fingers are closed around the interfaces;

4. EAU capture face is vertical, only two grippers fingers are closed around the interfaces.

The choice of the loads to be tested follows these considerations: the horizontal position was considered the most solid, as it is an axial-symmetrical position for linear motors; for this reason, fewer tests were conducted.

For the vertical position, on the other hand, it was considered necessary to better analyse the behaviour of the gripper because the lower fingers support most of the weight. For this reason, the tests have been performed with a fixed step of 0.2 kg. This was even more important for tests where only the bottom fingers of the gripper tightened the interfaces. The chosen step was 0.1 kg.

Test ID	**Weight** [kg]							
1	0.4	0.6	1.0	1.5				
2	0.4	0.6	0.8	1.0	1.2	1.4	1.6	
3-4	0.3	0.4	0.5	0.6	0.7	0.8	0.9	1.0

Table 4.1. Weights tested in the capture and holding test of SMACK.

All tests have been successfully passed but completed without finding the actual maximum load tolerated by the gripper. The test with a load of 1.6 kg was considered more than satisfactory, since it represents four times the expected maximum weight of the EAU. This choice is made to avoid damaging the components involved.

A single motor has a theoretical max force (lifted) of 50 N and a max side load of 10 N. Due to its design, SMACK captures the EAU with a resulting force of $R = 3F \sin \alpha$ that results in approximately 86 N (see Fig. 4.1). This means that the maximum load supported by the three actuators is approximately 8.8 kg.

This measurement of gripping force is underestimated because the friction that can help the finger hold the EAU was not taken into account.

The torques applied to the anchor point of the gripper are an estimation and are shown in Fig. 4.1. The location of the centre of mass is not known, but it is reasonable to assume that it is greatly influenced by the weight of the battery pack. To estimate the torque due to the weight of the EAU with respect to the anchor point, the values of the distances from the axis of rotation (b_1 and b_2

in Fig. 4.1) are estimated in excess of the estimated position of the centre of mass. The torque value in horizontal position and in vertical configurations are approximately:

$$M_1 = F_{Weau} \cdot b_1 = (0.4\ \text{kg} \cdot 9.81\ \text{m/s}^2) \cdot 0.1\ \text{m} = 0.4\ \text{Nm}$$
$$M_2 = F_{Weau} \cdot b_1 = (0.4\ \text{kg} \cdot 9.81\ \text{m/s}^2) \cdot 0.05\ \text{m} = 0.2\ \text{Nm}$$

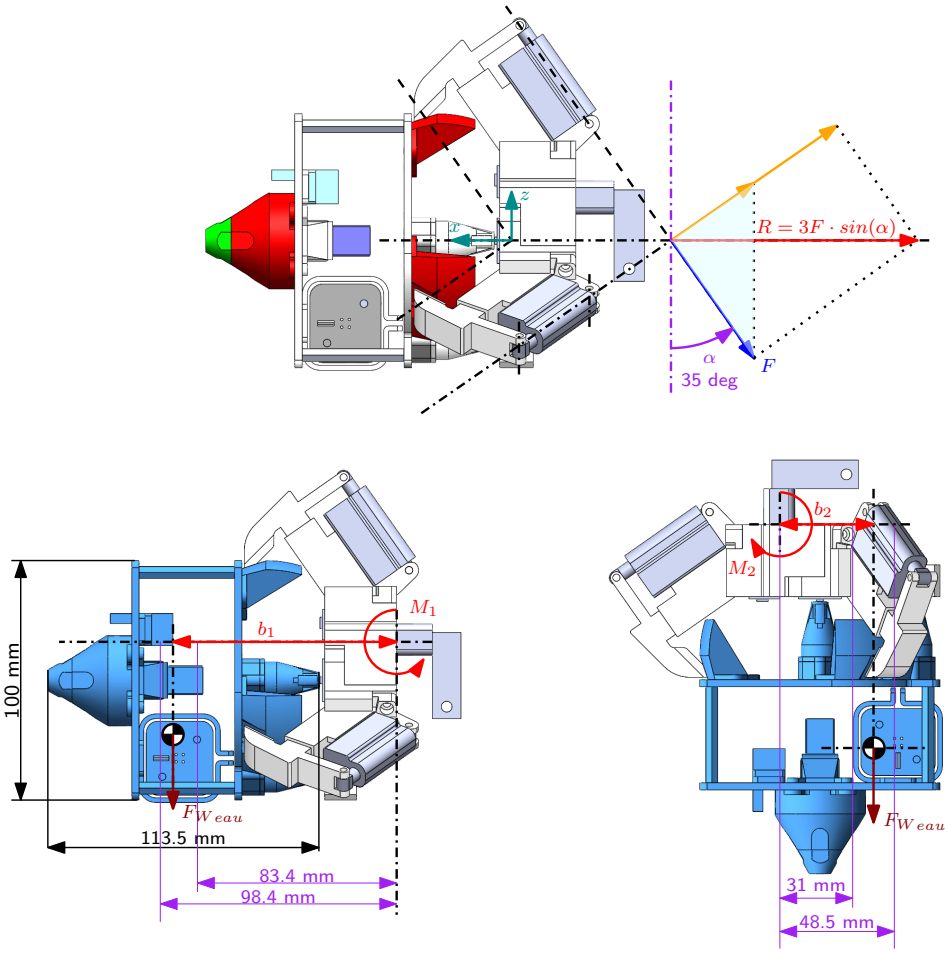

Figure 4.1. Diagram of gripper capture force and of the torques applied at the anchor point.

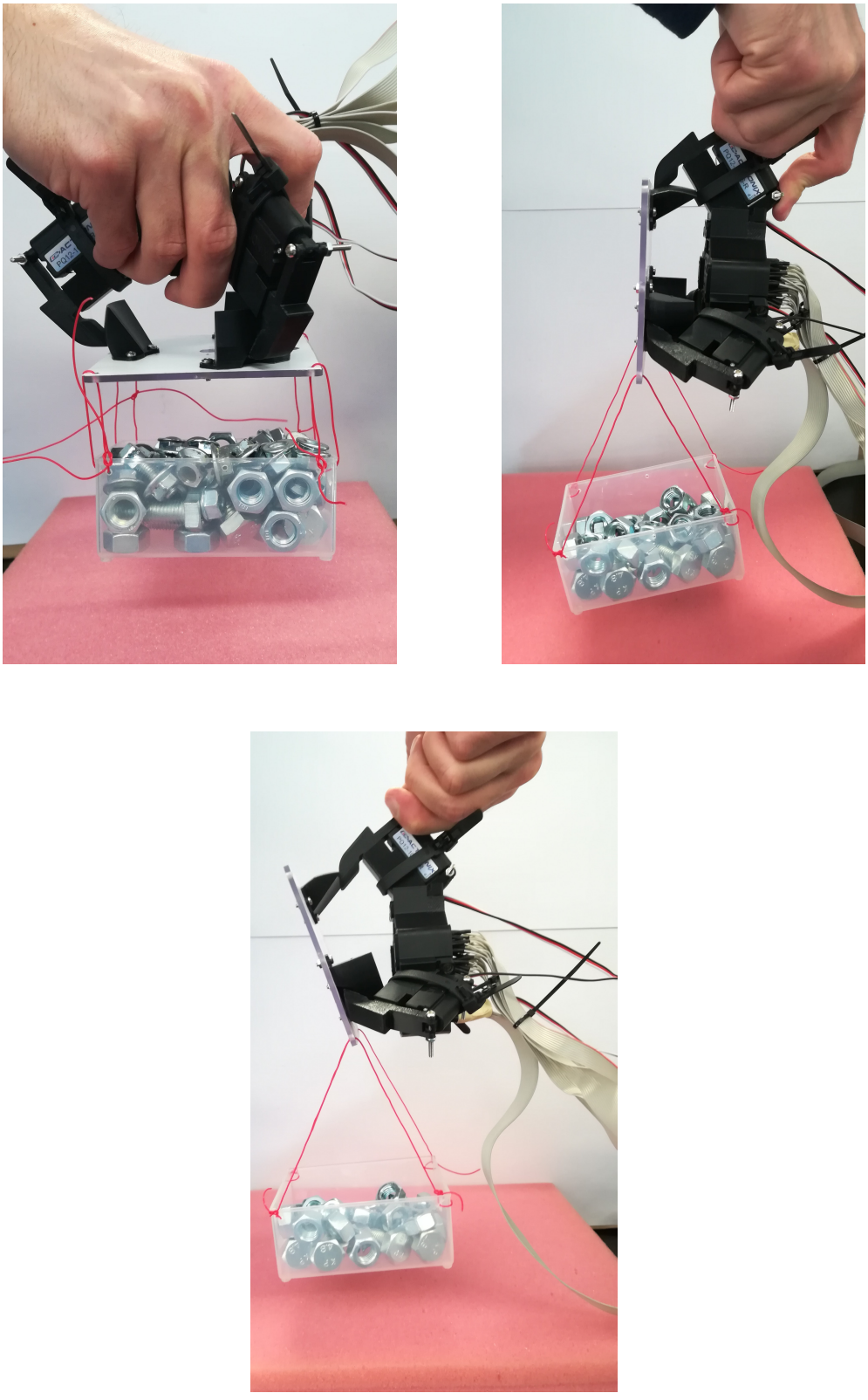

Figure 4.2. Overview of the placements tested in the capture and holding test.

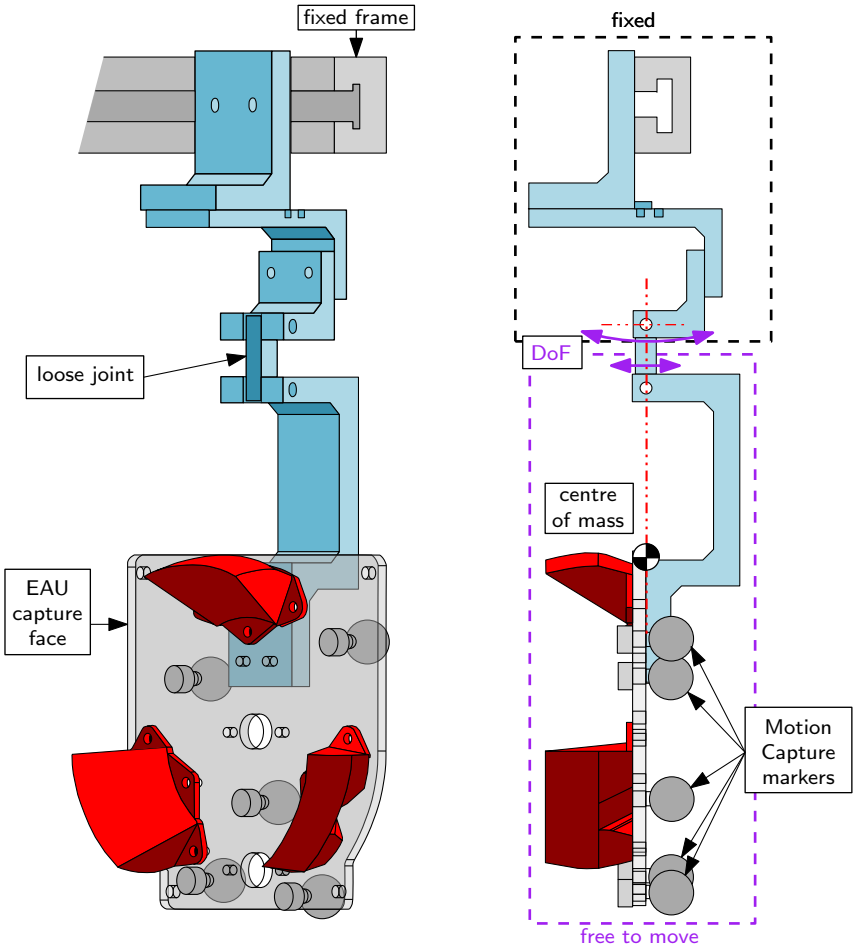

Figure 4.3. CAD model of the loose joint implemented for misalignment tests.

4.1.2 SMACK Misalignment tests

The purpose of these tests is to find the misalignments tolerated by SMACK that allow to perform a nominal capture (i.e. the fingers fit correctly in the slots of the capture interfaces to establish a rigid connection between SMACK and the EAU). The aim is to compare these values with the measurement errors of the sensors. To do this, the capture of the EAU capture face is done by forcing the alignment error in all the following degrees of freedom:

- Displacements along the y and z axis;
- Rotations around the x axis (roll), the y axis (pitch) and the z axis (yaw).

The robotic arm acts as a positioning system. To prevent collisions between SMACK and the EAU capture face, the latter is mounted on a fixed frame by means of a loose joint: this enables movements along the x axis and the yaw

rotation during the approach and capture by SMACK. It also allows to highlight collisions if they occur.

The loose joint is depicted in Fig. 4.3. Its peculiarity is that it also ensures that the EAU capture face remains perpendicular to the ground. This is obtained because the centre of mass of the face of the EAU is aligned with the rotation axis of the joint.

The test set-up and procedure are as follows:

- SMACK is mounted on the end-effector of the robotic arm and the EAU capture face on the fixed frame by means of the loose joint;
- A first capture is executed in order to set the capture position;
- SMACK is then retracted in the $-x$ direction of the amount of 50 mm;
- A displacement or rotation is imposed with respect to the centre of the EAU capture face;
- SMACK is approached along the x direction by the previous amount of 50 mm;
- SMACK fingers are closed to capture the EAU capture face.

The results are reported in Tab. 4.2. The test is considered *passed* if SMACK does not hit the face and captures correctly, *partially passed* if SMACK hits the face but still captures, while *fail* if the gripper fingers do not enter in the concave slots of the capture interfaces (non-nominal catch).

Since the EAU capture face is symmetric with respect to the $x - z$ plane, the tests are performed only along the y direction and not in the $-y$ direction. The same consideration applies to rotation around the x and z axes.

On the other hand, tolerated misalignments in the z and $-z$ directions are not equivalent due to SMACK, which has only one finger at the top and two at the bottom. This implies that the tolerated misalignment in the z direction is greater than that in the opposite direction.

SMACK can also tolerate simultaneous misalignments in the y and z directions. These possible values are found as the intersection between the area of the circle with diameter $(z_{min} \div z_{max})$ and the area of the circle with diameter $(y_{min} \div y_{max})$. The area of possible mixed misalignments in y and z is shown in the Fig. 4.4.

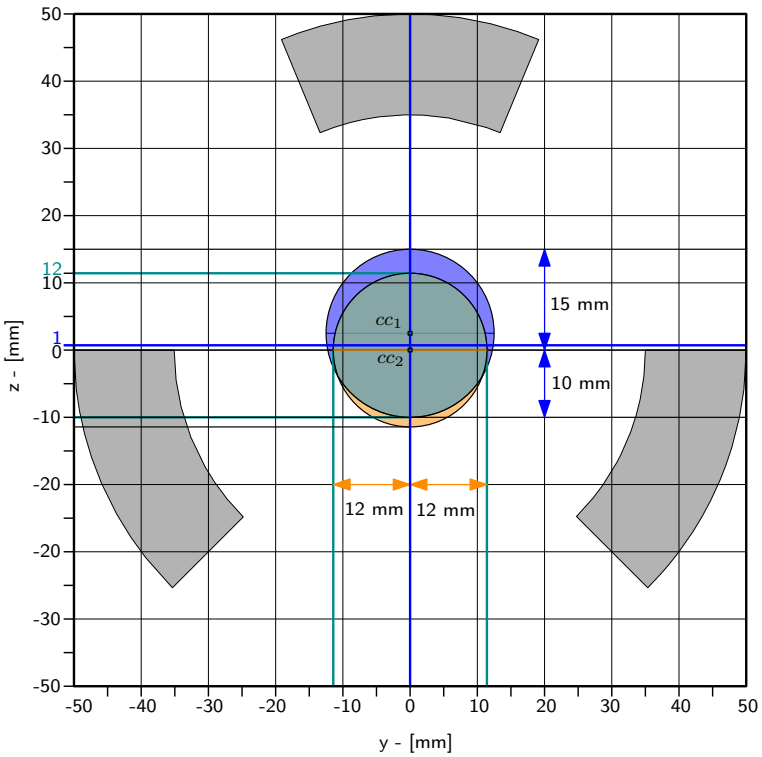

Figure 4.4. The misalignments in $y - z$ plane obtained with the tests.

axis	**displacement** [mm]	**Test result** Pass/Fail
y	5	Pass
y	8	Pass
y	10	Pass
y	12	Pass
y	13	Partially fail
y	14	Fail
z	5	Pass
z	10	Pass
z	15	Pass
z	18	Partially fail
z	20	Fail
z	-5	Pass
z	-10	Pass
z	-15	Fail

axis	**rotation** [deg]	**Test result** Pass/Fail
x	5	Pass
x	7	Pass
x	8	Pass
x	9	Pass
x	10	Partially fail
x	11	Fail
y	5	Pass
y	7	Fail
y	-5	Pass
y	-7	Fail
z	5	Pass
z	10	Pass
z	12	Partially fail
z	15	Partially fail
z	20	Fail

Table 4.2. The displacements and rotations imposed to the EAU capture face in order to find the amount of tolerated misalignments by SMACK.

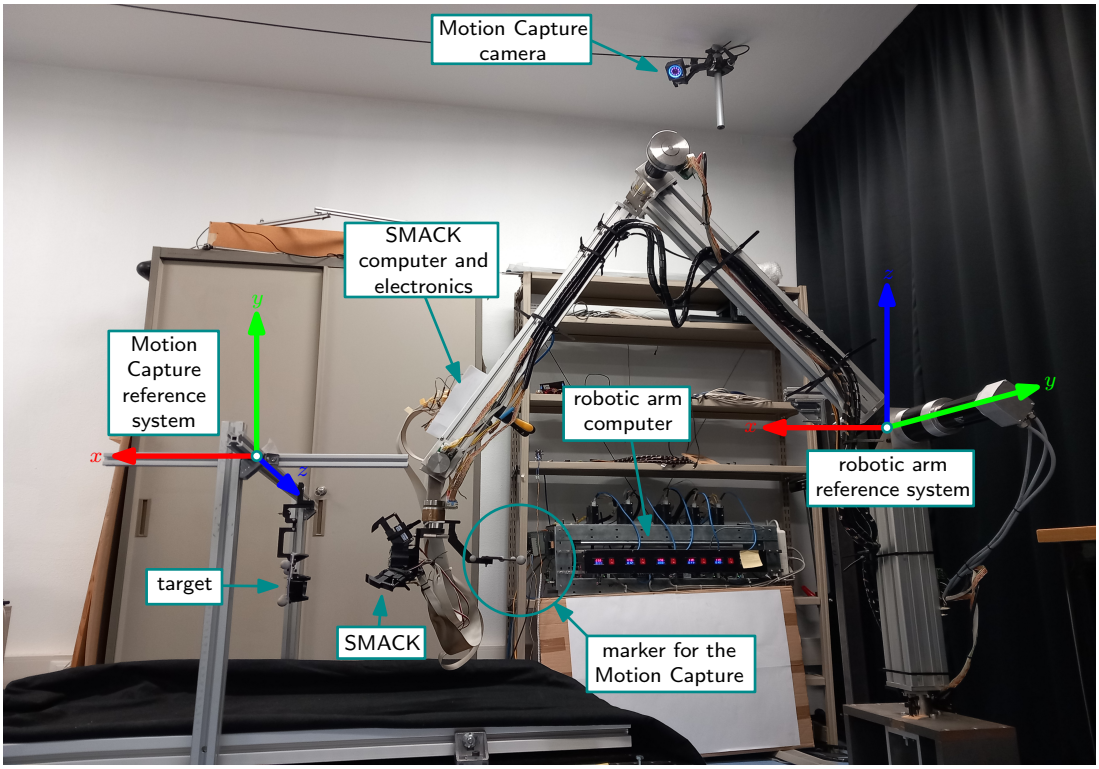

Figure 4.5. An image of the experimental set–up employed for the test campaign.

4.2 Measurement subsystem tests

4.2.1 Tests facility

The main idea of the SMACK design is that it will be mounted on a space robotic arm and will drive it to perform assembly operations. For this reason, to test the capabilities of SMACK, it has been mounted at the end-effector of a 6 Degree-of-Freedom robotic arm. The face of the EAU, instead, has been mounted on a fixed frame in the working area of the robotic arm (shown in Fig. 4.5). The robotic arm has been designed and tested to have an accuracy error that is sufficient to be used as a placing system to test the SMACK sensor suite [4], [5].

To have a reliable reference for the tests, a motion capture system (*Optitrak Prime 13x*) is placed at the corners of the work area. These collected data are used as ground truth to which compare the sensor estimation. It is composed of four cameras and records the position and attitude of spherical reflective markers, which are placed on SMACK and EAU to record their motion. The system tracks these markers with positional errors lower than ±0.20 mm, rotational errors lower than 0.5 deg and a sampling time of 0.0015 s.

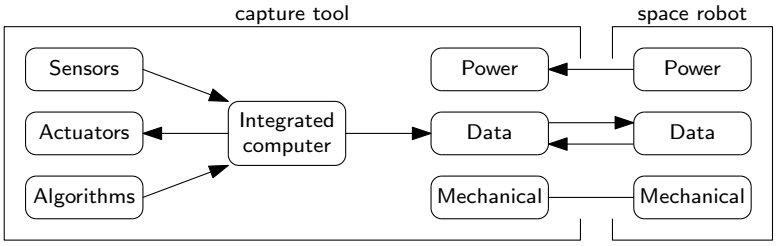

Figure 4.6. The schematic representation of the interfaces required between SMACK and robotic arm.

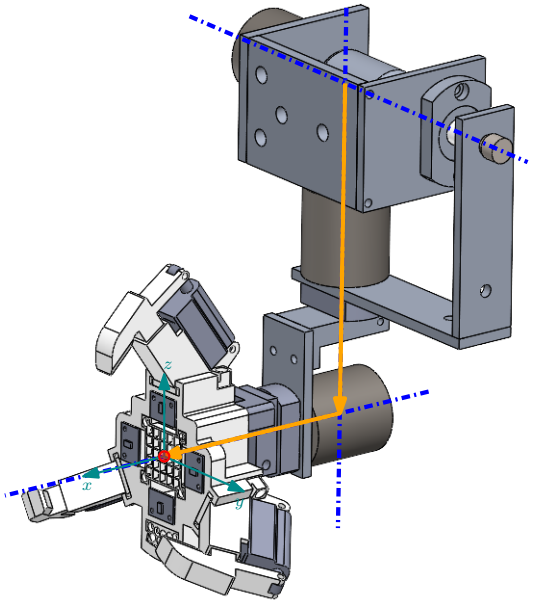

Figure 4.7. CAD model of the spherical manipulator. The robotic arm calculates the inverse kinematics starting from the desired position that the gripper centre has to reach with the desired attitude.

At the beginning of the test campaign, it is necessary to set the origin of its coordinate system and to align it with the one of the robotic arm. The two reference frames are reported in Fig. 4.5. The one chosen as the primary reference system is that of the robotic arm.

In Fig. 4.6 are shown the interfaces required between SMACK and the robotic arm. To allow SMACK to transmit the desired position, its computer is connected to the robotic arm computer via TCP/IP communication. The positions that SMACK transmits to the robotic arm are referred to its reference system; therefore, the centre of the matrix sensor (the red dot in Fig. 4.7). To position SMACK, the robotic arm solves the inverse kinematics starting from this point, due to the fact that the distances shown in Fig. 4.7 (the orange vectors) are

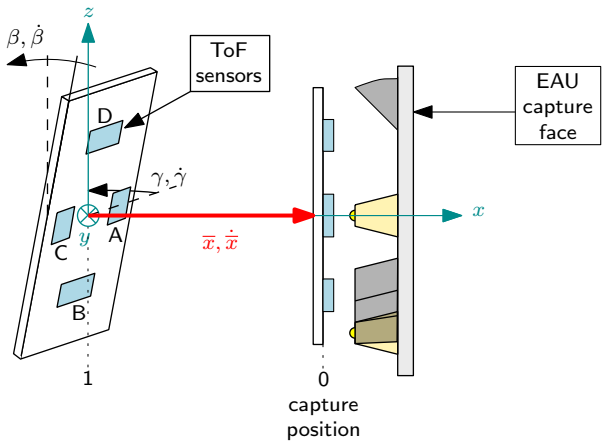

Figure 4.8. Schematic representation of dynamic tests performed to evaluate ToF estimation errors.

reported in the inverse kinematics algorithm.

In addition to the position, SMACK also transmits the time to execute the manoeuvre. This is used by the robotic arm to calculate the velocity of the end-effector and the velocity of the joints, with its inverse differential kinematics algorithm.

4.2.2 Estimation algorithm tests

To improve the EAU pose estimation performed with the ToF sensors, a model–based estimation algorithm has been implemented as explained in 3.2 in order to apply the Kalman filter.

Test procedure

The dynamic tests to evaluate the performance of the algorithm have been executed as follows (a schematic representation in Fig. 4.8):

1. A zeroing procedure is performed when SMACK captures the EAU in order to set the zero of the motion capture;

2. From the zero position, depending on the tests, the robotic arm places SMACK in several positions with respect to the EAU and performs different manoeuvres;

3. The Kalman filter algorithm estimates the distance along the x axis, the pitch and the yaw angles, and the relative rates with a sampling time $\Delta t = 0.05\,\text{s}$ (used in Eq. 3.10);

4. At the same time, the motion capture system records the position between SMACK and the EAU. The reference velocity is computed as the discrete derivative between two consecutive positions;
5. The errors are obtained as the absolute value of the difference between the reference position and velocity (from the motion capture) and the estimated quantities.

Test results

In total, fourteen different dynamic tests were performed with an increasing level of complexity: tests of elementary movements and tests with combined movements executed with a given velocity. To present their results, they are divided into four groups:

- **Group A**: approach manoeuvre in aligned attitude;
- **Group B**: simple rotations at a fixed distance from the face;
- **Group C**: approach manoeuvre and simultaneous rotation;
- **Group D**: approach manoeuvre and two simultaneous rotations.

In Tabs. 4.3, 4.4, 4.5 and 4.6 the type of test and errors are summarised.

Test ID	Involved DoF	Manoeuvre param. range [mm]	time [s]	velocity [mm/s]	Position Error avg. [mm]	σ [mm]	Velocity Error avg. [mm/s]	σ [mm/s]
A.1	x	100÷0	10	10	1.44	1.03	1.52	2.14
A.2	x	90÷0	10	9	1.00	0.84	1.42	1.64
A.3	x	90÷0	5	18	1.58	1.15	3.31	3.82
A.4	x	90÷0	2	45	2.21	2.14	8.30	9.41
				average error	**1.56**	**1.29**	**3.14**	**4.25**

Table 4.3. Approach along the x axis (1 DoF test) with different approaching velocity and the resulting estimation errors for the kalman filter test.

Group A The first type of tests is the approach along the x direction: as visible in Tab. 4.3 and in Figs. 4.9 to 4.12, different manoeuvre times have been considered to evaluate the performance of the Kalman filter in estimating the velocities.

The average error on the estimated position is 1.56 mm and the error on the estimated velocity is 3.14 mm/s.

As reported in Tab. 4.3, this is due to the fact that as the manoeuvring time decreases, the speed estimation error increases considerably. This is because the Kalman filter needs several iterations to converge. The test where the approach manoeuvre is performed in 2 s (Fig. 4.12) shows this behaviour: the Kalman filter fails to estimate the speed because the movement is too fast. Therefore, it was decided to keep 5 s as the lower manoeuvre time limit.

In Figs. 4.9 to 4.12 it is also possible to observe that the initial estimated position has a higher error than during the approach manoeuvre. This is visible in all tests performed, even in tests where a shorter distance from the EAU was considered. This is due to the fact that the Kalman filter needs some iterations and measurements to converge.

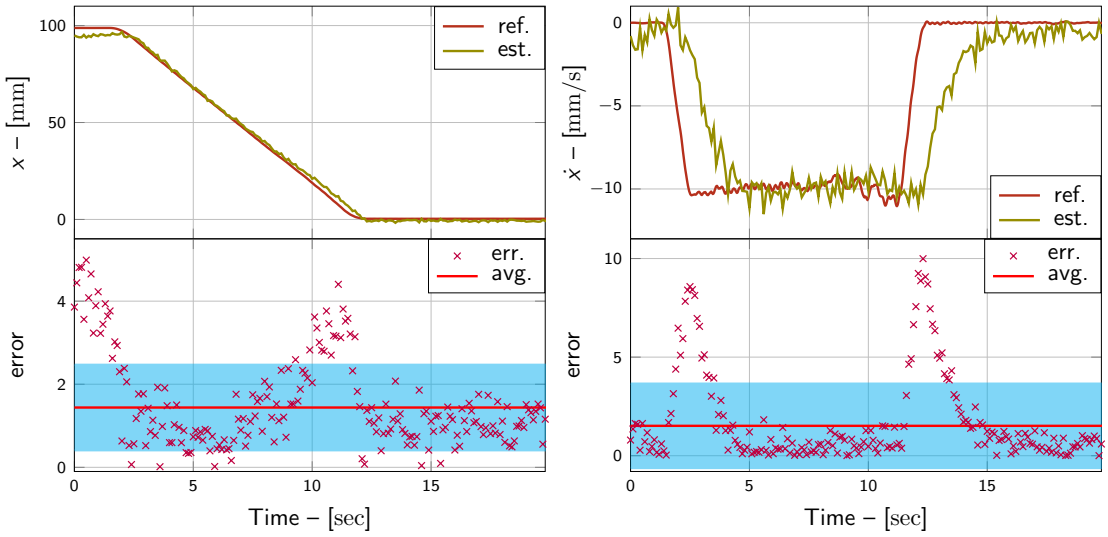

Figure 4.9. Kalman Filter Test (A.1): SMACK goes from a distance of 100 mm from EAU to 0 in 10 s (approach velocity is 10 mm/s).

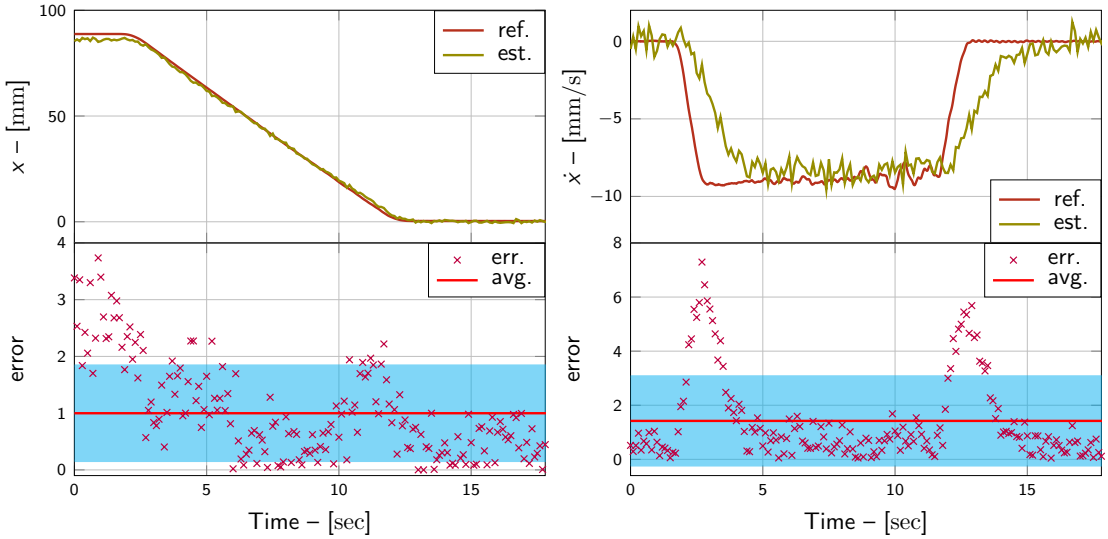

Figure 4.10. Kalman Filter Test (A.2): SMACK goes from a distance of 90 mm from EAU to 0 in 10 s (approach velocity is 9 mm/s).

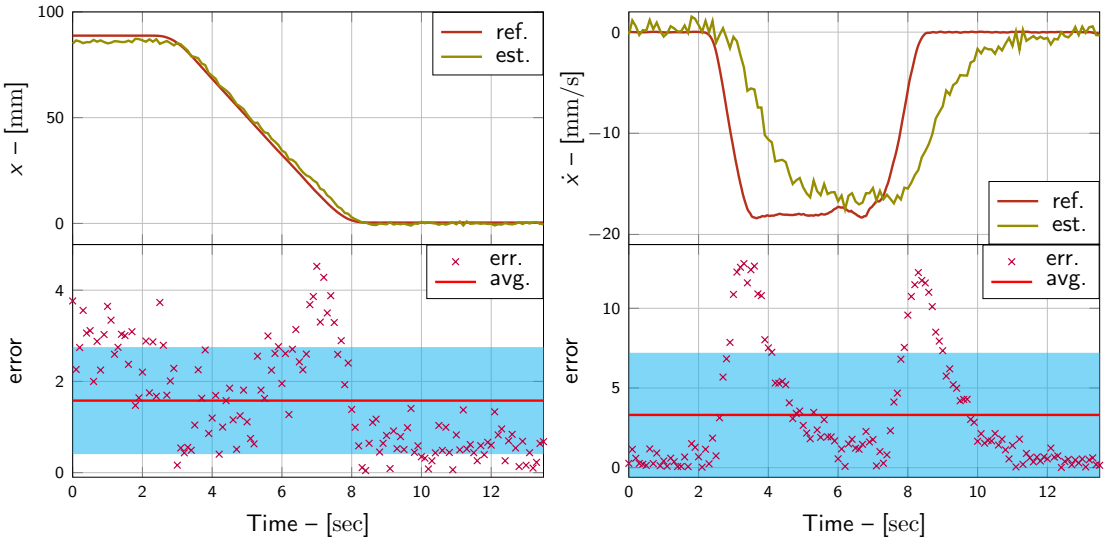

Figure 4.11. Kalman Filter Test (A.3): SMACK goes from a distance of 100 mm from EAU to 0 in 5 s (approach velocity is 18 mm/s).

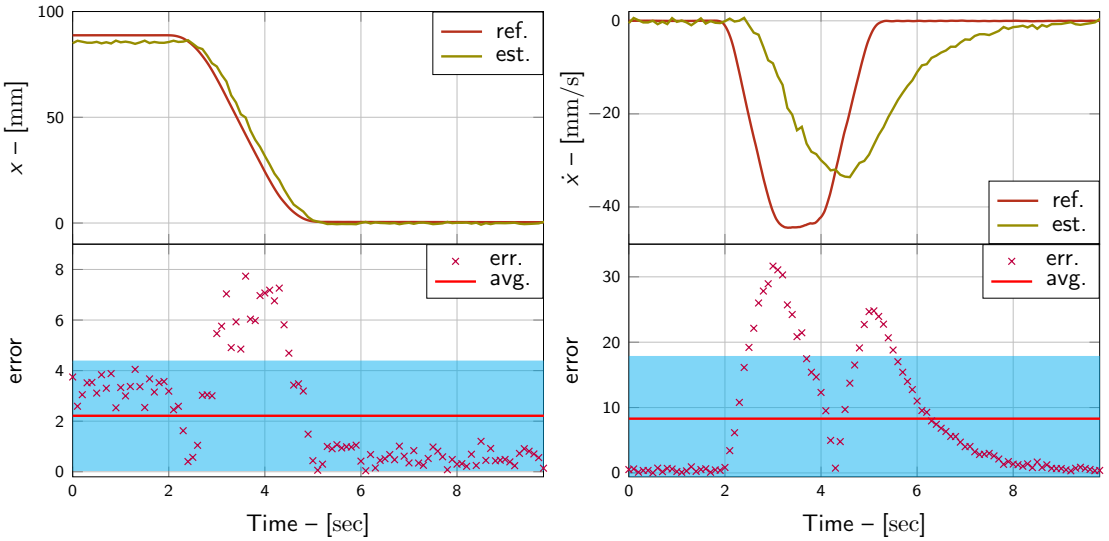

Figure 4.12. Kalman Filter Test (A.4): SMACK goes from a distance of 100 mm from EAU to 0 in 2 s (approach velocity is 45 mm/s).

Test ID	Involved DoF	Manoeuvre param. range [deg]	time [s]	velocity [deg/s]	Position Error avg. [deg]	σ [deg]	Velocity Error avg. [deg/s]	σ [deg/s]
B.5	pitch	-20÷20	10	4	5.35	3.35	2.21	1.87
B.6	pitch	-20÷20	5	8	9.86	5.11	1.91	1.98
B.7	yaw	-15÷15	10	3	1.48	1.04	1.14	0.86
B.8	yaw	-15÷15	5	6	1.68	1.22	1.25	0.98
				average error	**4.59**	**2.68**	**1.63**	**1.42**

Table 4.4. Single rotations around the y and z axis (1 DoF test) with different manoeuvre time and the resulting estimation errors for the kalman filter test.

Group B The second type of tests are simple rotations around the y and z axes, and the main results are shown in Tab. 4.4 and in Figs. 4.13 to 4.14.

The robotic arm rotates SMACK, always keeping the centre of the gripper aligned with the centre of the EAU. In these tests, the negative effect of vibrations is visible, which causes the Kalman filter estimation to diverge at those points.

The average error on the estimated position is 4.59 deg against that of the estimated velocity, which is 1.63 deg/s.

This angular estimation error for pitch angle estimation is due to the choice of angular range to sweep: using [-20÷20] deg leads to major errors because the face is not in the ToF field of view. If the swept angle is reduced, choosing an initial value of 15 deg instead of 20 deg in yaw angle tests, it is possible to notice a considerable reduction of the error. The average error goes from 5.35 deg to 1.48 deg for the 10 s manoeuvre, and from 9.86 deg to 1.68 deg for the 5 s manoeuvre. Therefore, 15 deg is considered the limit for the ToF and the Kalman filter.

These test manoeuvre values (range, time) are accurately used to better understand the model and identify its limits. In any case, such a large amount of rotation in Close-Proximity operations is well beyond acceptable values. Having said that, the gripper is capable of handling up to 10 deg of misalignment along z, and this rotation value was chosen for the next group of tests as the maximum value.

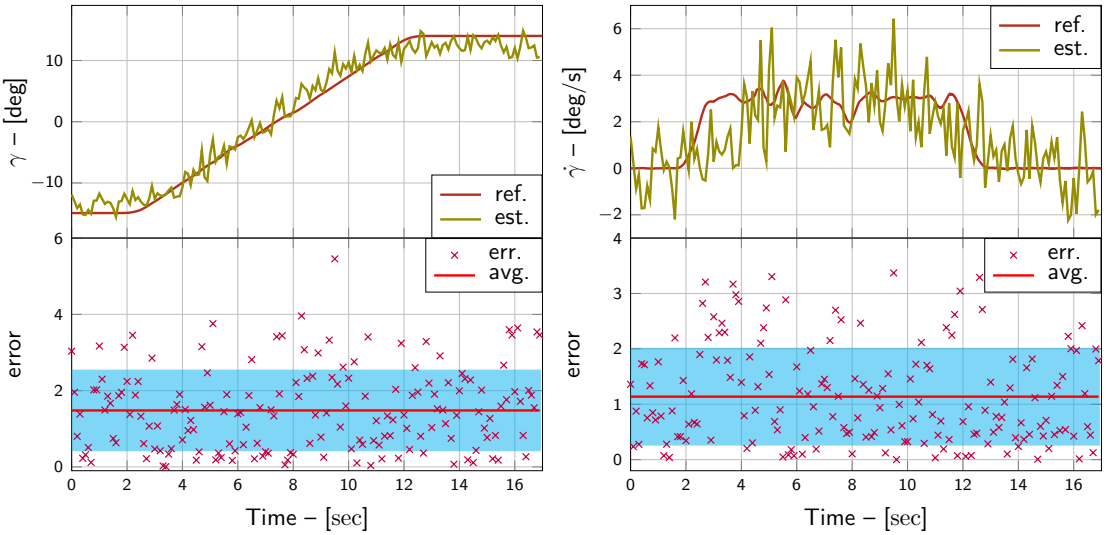

Figure 4.13. Kalman Filter Test (B.7): SMACK sweeps a yaw angle ranging from −15 deg to 15 deg in 10 s (angle rate is 3 deg/s). SMACK and EAU are 50 mm apart constantly.

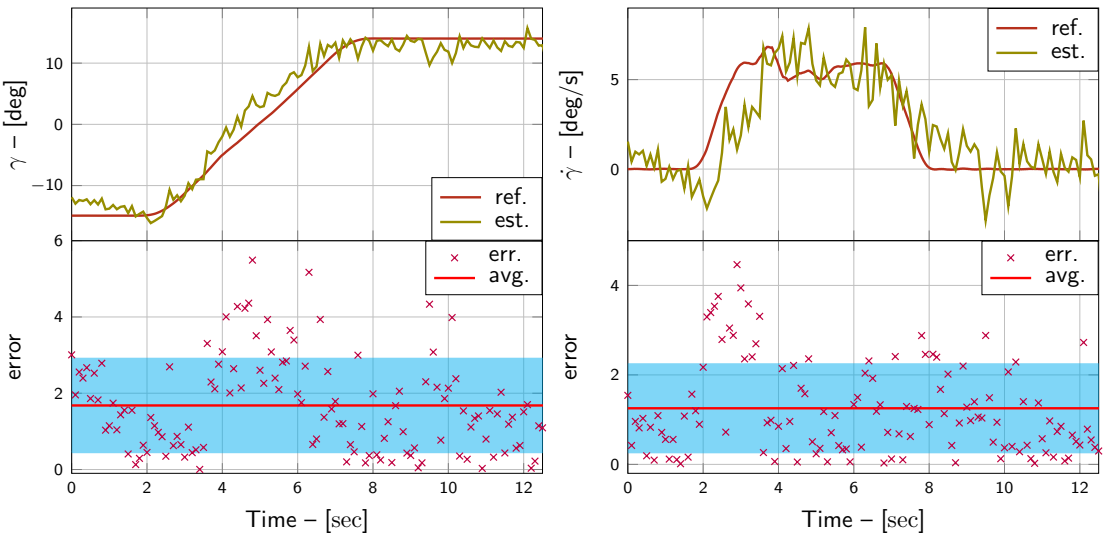

Figure 4.14. Kalman Filter Test (B.8): SMACK sweeps a yaw angle ranging from −15 deg to 15 deg in 5 s (angle rate is 6 deg/s). SMACK and EAU are 50 mm apart constantly.

Test ID	**Involved DoF**	**Manoeuvre param.**			**Position Error**		**Velocity Error**	
		range	**time** [s]	**velocity**	**avg.**	σ	**avg.**	σ
C.9	x	80÷0	10	8	1.32	1.13	1.70	1.68
	yaw	-10÷0		1	1.56	1.22	1.14	0.93
C.10	x	80÷0	5	16	1.67	1.49	1.91	2.28
	yaw	-10÷0		2	1.11	0.88	1.01	0.75
C.11	x	80÷0	10	8	1.98	1.53	1.21	1.48
	pitch	-10÷0		1	1.49	1.19	1.27	0.91
C.12	x	80÷0	5	16	0.89	0.80	2.29	2.43
	pitch	-10÷0		2	2.08	1.18	2.28	1.22
average distance error					**1.46**	**1.24**	**1.78**	**1.97**
average attitude error					**1.56**	**1.12**	**1.43**	**0.95**

Table 4.5. Approach manoeuvre with a single rotations around the y or z axis (2 DoF test) with different manoeuvre time and the resulting estimation errors for the kalman filter test. The unit of measurement relative to the x are in mm and mm/s, while the unit of measurement relative to the pitch and yaw angle are in deg and deg/s.

Group C The third type of test consists of a simultaneous approach and a single rotation manoeuvre, both around y or in z, at different manoeuvre times. The results are shown in Tab. 4.5 and Figs. 4.15 to 4.18.

With all of the above considerations, it can be seen that, despite combined motion, the error in angle and estimated velocity is always within the misalignment limits accepted by the gripper.

The average error in the estimated distance is 1.46 mm and the one on the estimated velocity is 1.78 mm/s. The average error on the estimated attitude is 1.56 deg and the one on the estimated velocity is 1.43 deg/s.

As in Figs. 4.15 to 4.18, the highest estimation errors on the velocities are at the beginning and at the end of the motion. This is because the algorithm needs more measurements to estimate a varying velocity. However, it is noted that after the initial error, the Kalman filter tends to follow the trend of the reference data of the Motion Capture system.

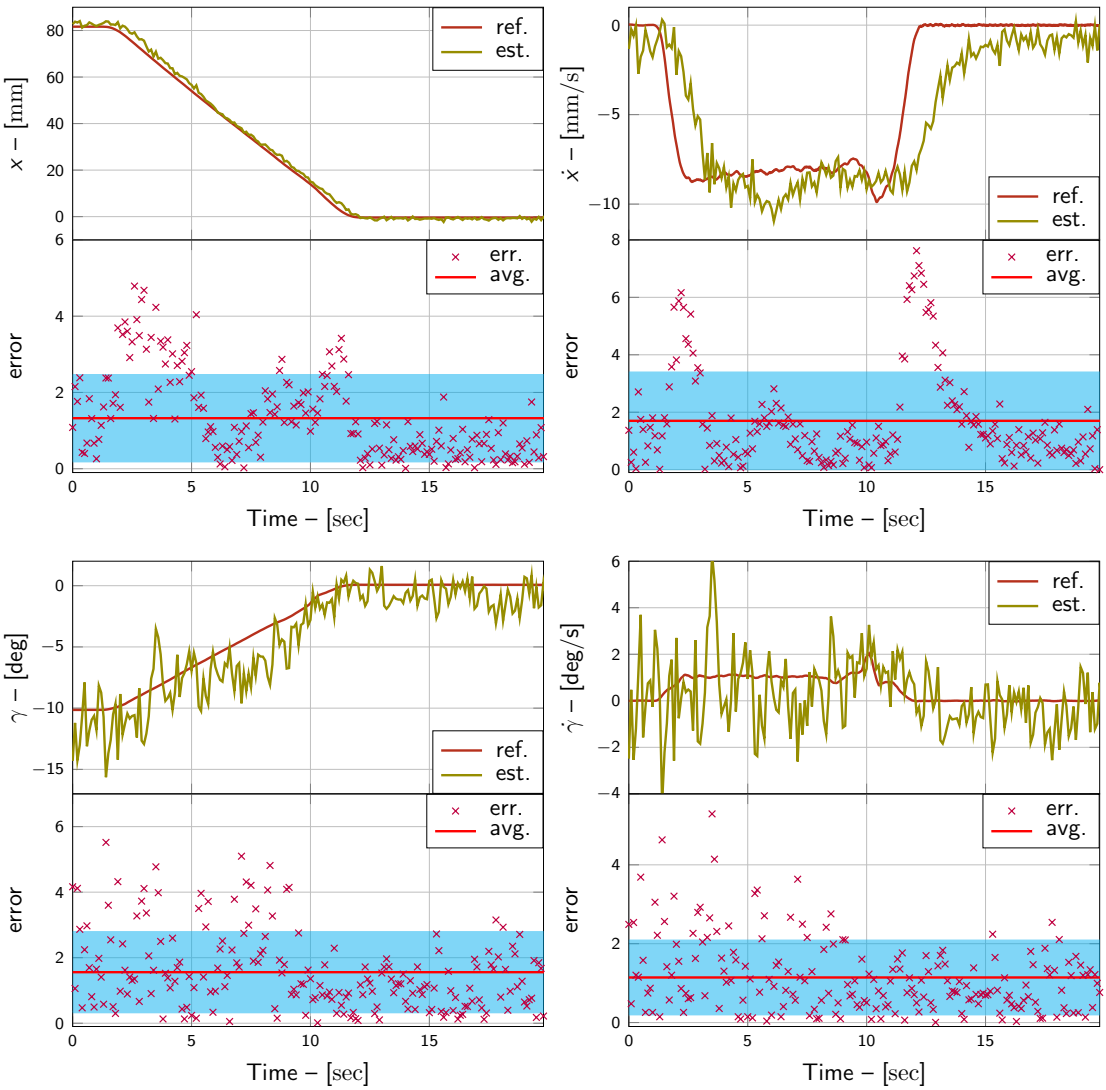

Figure 4.15. Kalman Filter Test (C.9): SMACK approaches the EAU from a distance of 80 mm up to 0 mm while rotating from −10 deg to 0 deg around the z axis. The manoeuvre lasts 10 s.

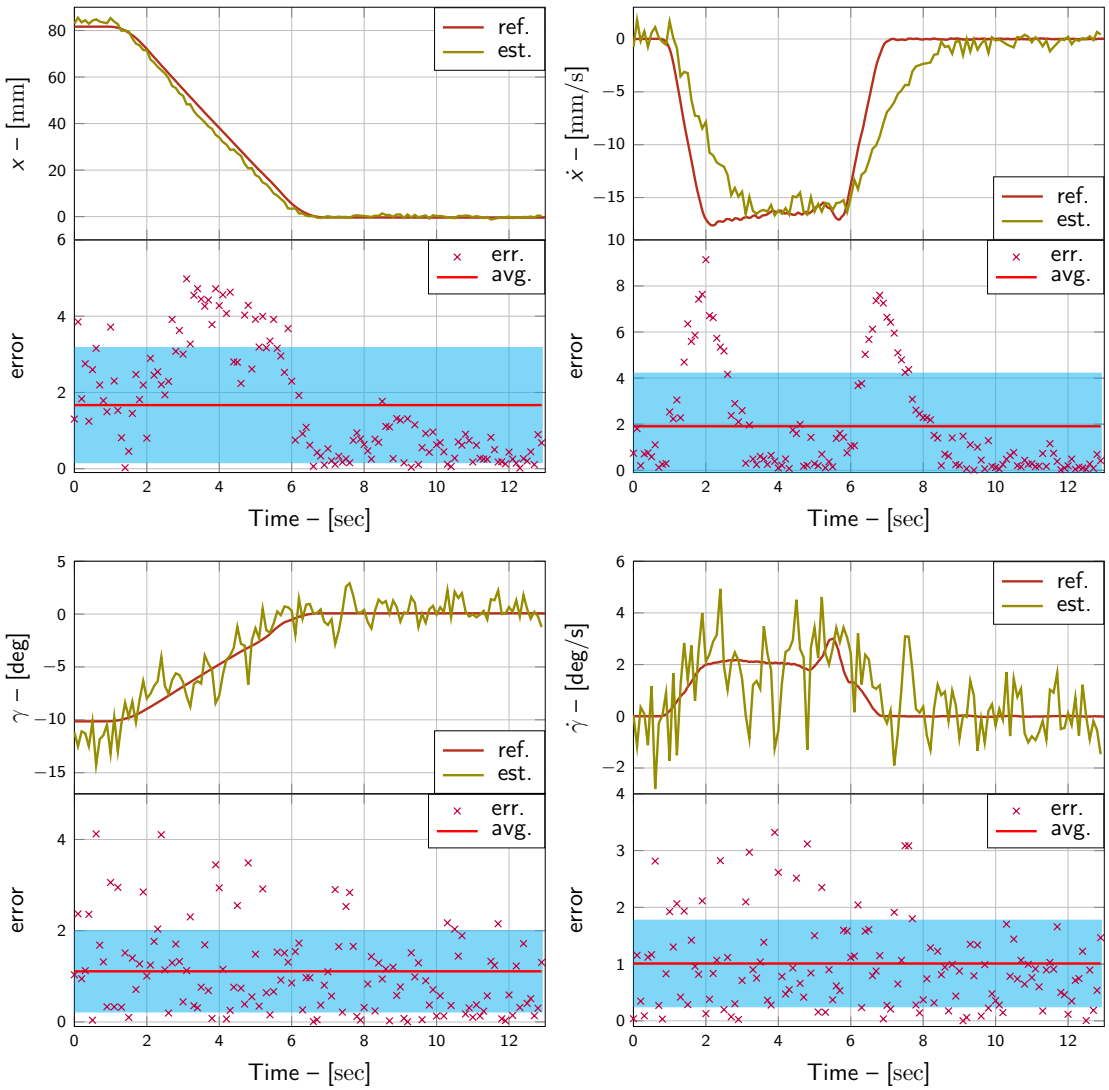

Figure 4.16. Kalman Filter Test (C.10): SMACK approaches the EAU from a distance of 80 mm up to 0 mm while rotating from −10 deg to 0 deg around the z axis. The manoeuvre lasts 5 s.

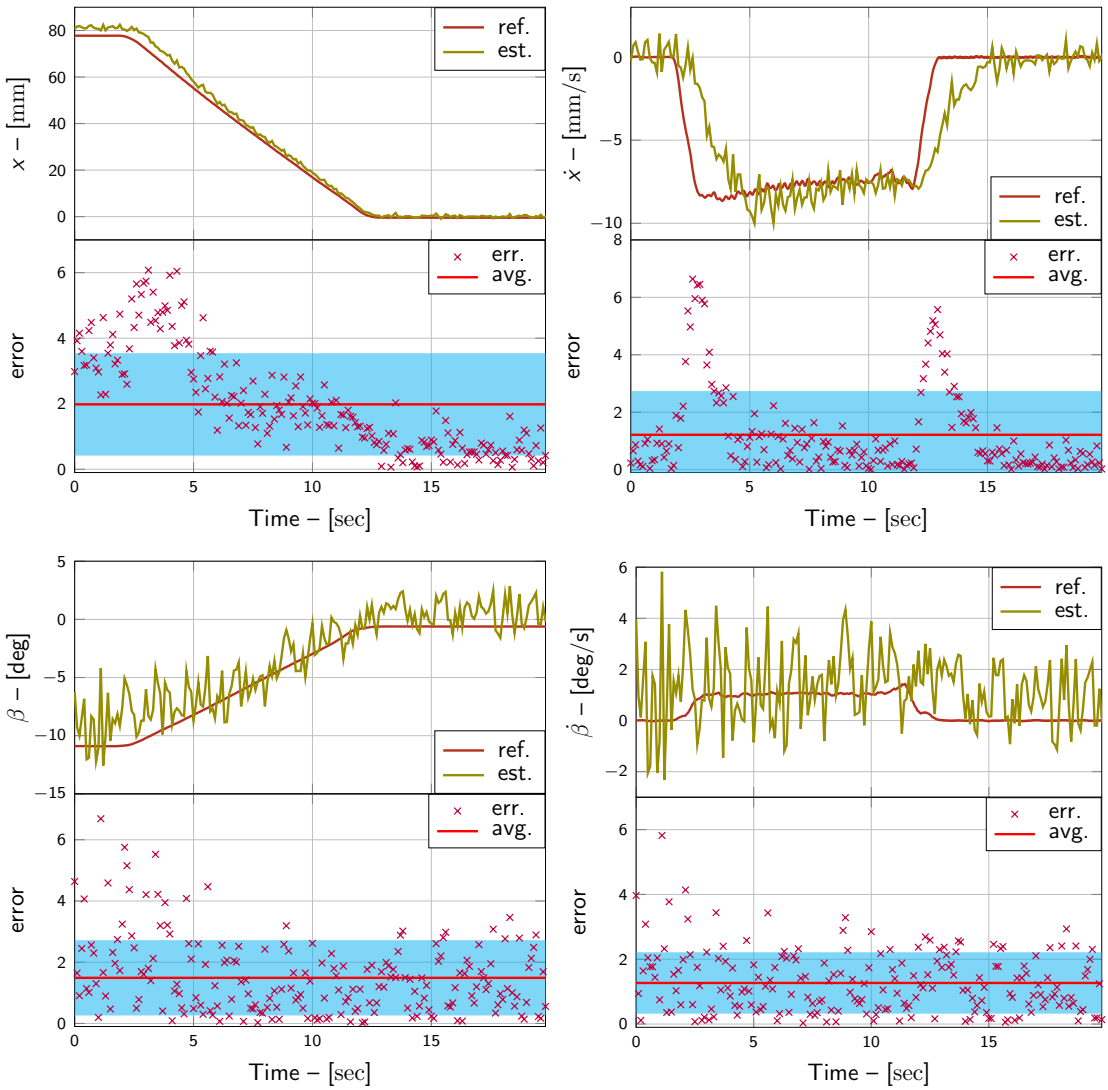

Figure 4.17. Kalman Filter Test (C.11): SMACK approaches the EAU from a distance of 80 mm up to 0 mm while rotating from −10 deg to 0 deg around the y axis. The manoeuvre lasts 10 s.

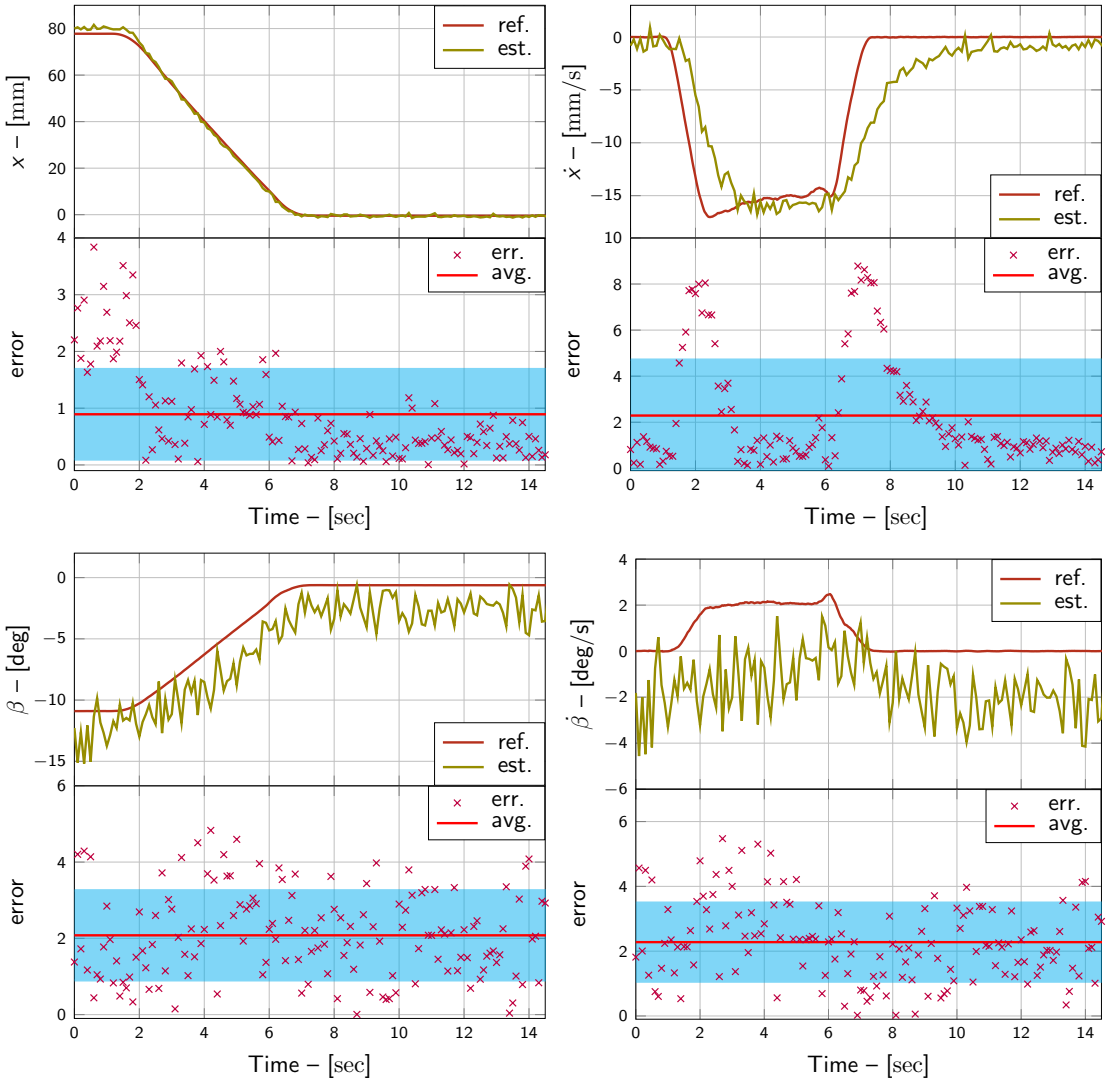

Figure 4.18. Kalman Filter Test (C.12): SMACK approaches the EAU from a distance of 80 mm up to 0 mm while rotating from −10 deg to 0 deg around the y axis. The manoeuvre lasts 5 s.

Test ID	Involved DoF	Manoeuvre param.			Position Error		Velocity Error	
		range	**time** [s]	**velocity**	**avg.**	σ	**avg.**	σ
D.13	x	80÷0	10	8	0.82	0.73	1.07	1.16
	pitch	-10÷0		1	1.37	0.96	0.96	0.82
	yaw	10÷0		1	2.03	2.05	1.04	0.87
D.14	x	80÷0	5	16	1.73	1.84	2.70	3.45
	pitch	-10÷0		2	2.48	1.49	1.40	1.02
	yaw	10÷0		2	1.89	1.47	1.82	1.40
average distance error					**1.28**	**1.29**	**1.89**	**2.31**
average attitude error					**1.94**	**1.49**	**2.61**	**1.03**

Table 4.6. Approach manoeuvre with both rotations around the y and z axis (3 DoF test) performed at different manoeuvre time and the resulting estimation errors for the kalman filter test. The unit of measurement relative to the x are in mm and mm/s, while the unit of measurement relative to the pitch and yaw angle are in deg and deg/s.

Group D The last tests consist of an approach along the x direction while performing two simultaneous rotations, of the same magnitude, around the y and z axes. This manoeuvre is performed at different manoeuvre times. Eventually, up to 3 degrees of freedom are considered. The results are shown in Tab. 4.6 and Figs. 4.19 and 4.20.

All the considerations made for the previous cases are visible. Despite the combined motions, the errors are within the misalignment range tolerated by SMACK. The average error in the estimated distance is 1.28 mm and the one in the estimated velocity is 1.89 mm/s. The average error on the estimated attitude is 1.94 deg and the one on the estimated velocity is 2.61 deg/s.

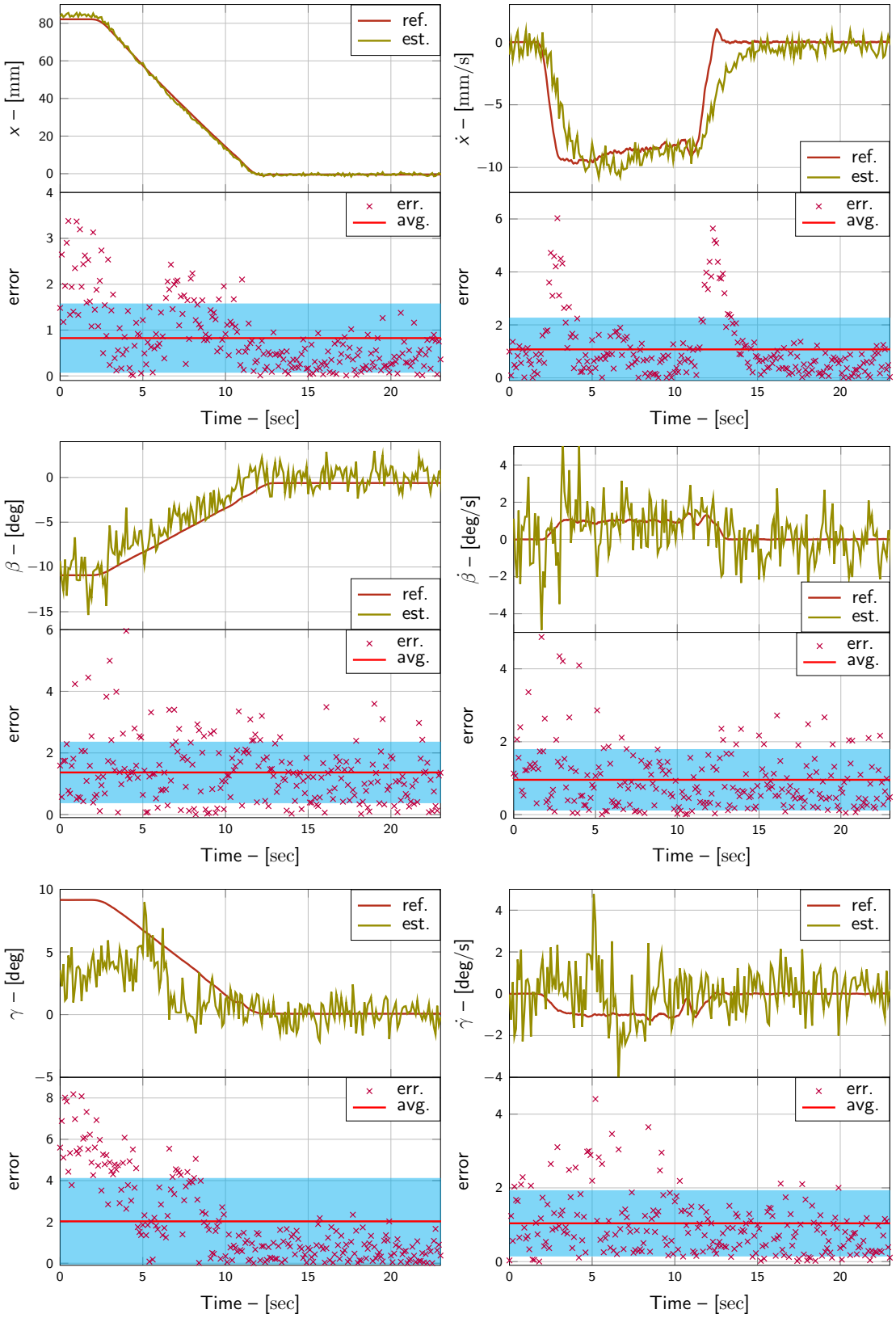

Figure 4.19. Kalman Filter Test (D.13): SMACK approaches the EAU from a distance of 80 mm up to 0 mm while rotating from −10 deg to 0 deg around the y axis and from 10 deg to 0 deg around the z axis. The manoeuvre lasts 10 s.

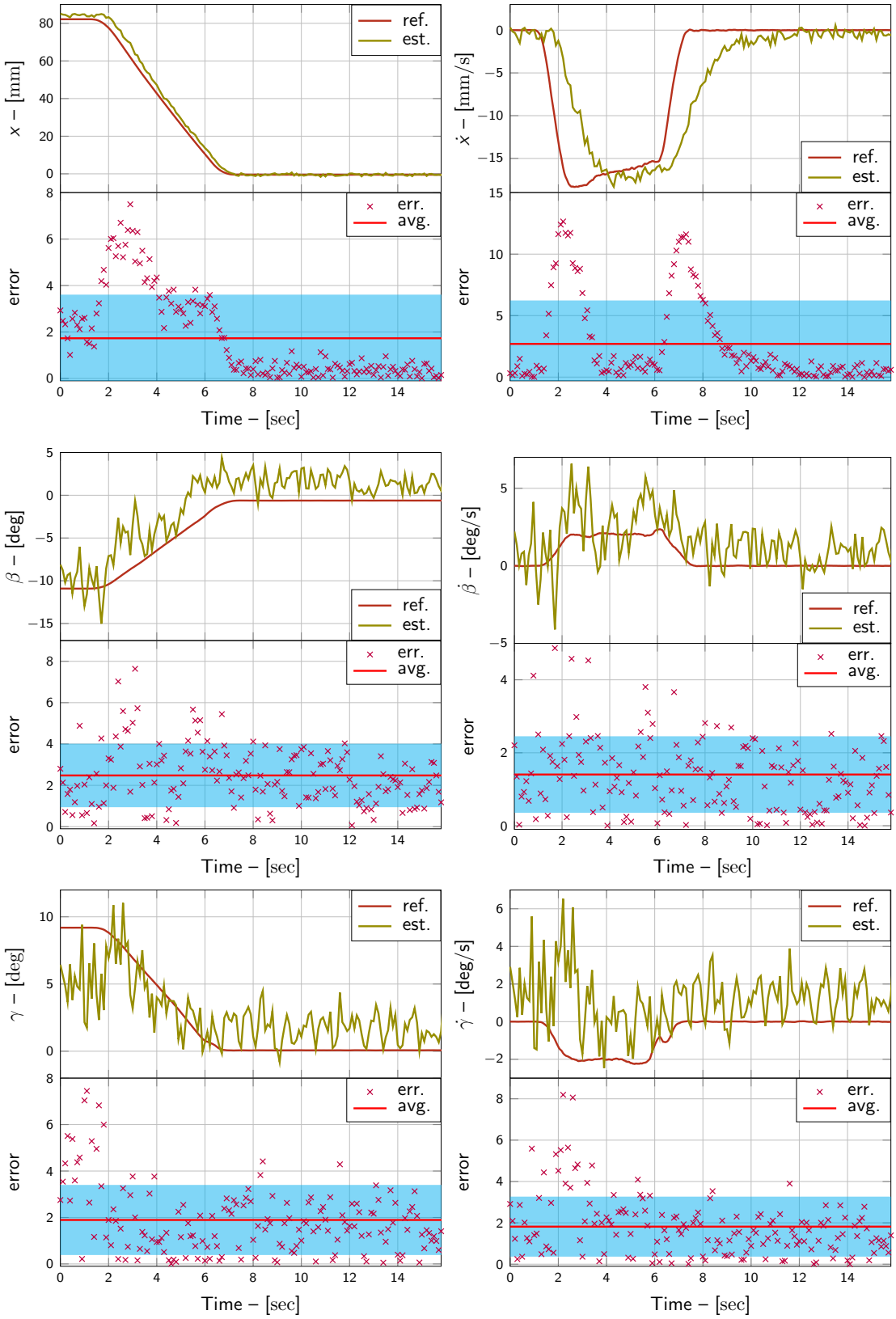

Figure 4.20. Kalman Filter Test (D.14): SMACK approaches the EAU from a distance of 80 mm up to 0 mm while rotating from −10 deg to 0 deg around the y axis and from 10 deg to 0 deg around the z axis. The manoeuvre lasts 5 s.

4.2.3 In-plane matrix sensor tests

The in-plane matrix can calculate the distance along the x direction and the position in the $y - z$ plane, based on the number of phototransistors activated by the LED placed on the EAU capture face. To test its performance, both the measurements have been tested. The matrix performs a measurement every 0.05 s and the data collected are compared with those of the Motion Capture system.

Measurement along the x direction

To test the measurement along the x direction, three tests are performed. The procedure is conceptually represented in Fig. 4.21 and is as follows:

- SMACK is mounted on the end-effector of the robotic arm and the EAU capture face is mounted on a fixed frame;
- A first capture is performed to set the motion capture to zero;
- SMACK is then retracted in the $-x$ direction of 70 mm;
- SMACK approaches the EAU position with different manoeuvre times, while the matrix sensor saves the data for post-processing and the motion capture records the relative position.

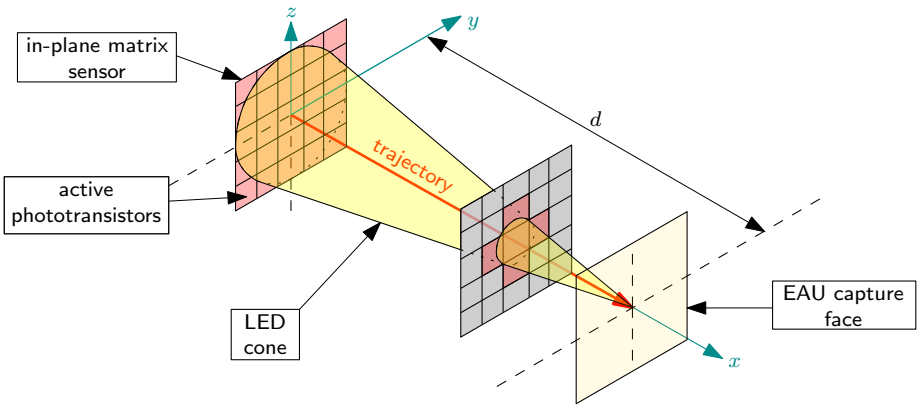

Figure 4.21. Schematic representation of test performed on the in-plane matrix to evaluate distance estimation errors.

The tests results are reported in Tab. 4.7 and in Fig. 4.22. They show that the sensor measures the relative position with a step behaviour due to its discrete nature (phototransistors are spaced by 5 mm).

The main performance parameters are as follows:

- **Maximum operating distance** 40 mm

  At this distance, all phototransistors are activated by the LED cone, and the sensor is not able to reconstruct the position beyond 40 mm.

- **Accuracy**

  The matrix exhibits a piece-wise behaviour:

  - From a distance between $[0 \div 20]$ mm the average accuracy is 2 mm;
  - From a distance between $[20 \div 40]$ mm the average accuracy is 4 mm. In this range, the errors increase.

- **Average error** 4.69 mm

  Calculated in the distance range $[0 \div 40]$ mm from the EAU. The number of activated phototransistors changes with an average of 2.5 mm along the x axis, and its accuracy improves as the distance between the matrix sensor and the LED decreases.

Different manoeuvre times are evaluated, but no significant influences on the estimation are observable.

Test ID	**Distance** x [mm]	**Manoeuvre time** [s]	**Error**	
			avg. [mm]	σ [mm]
1	$70 \div 0$	5	4.88	5.73
2	$70 \div 0$	3	4.69	5.31
3	$70 \div 0$	2	4.49	5.55
		average error	**4.69**	**5.53**

Table 4.7. Values characterizing the approach tests along the x direction and the resulting estimation errors for the in-plane matrix sensor test.

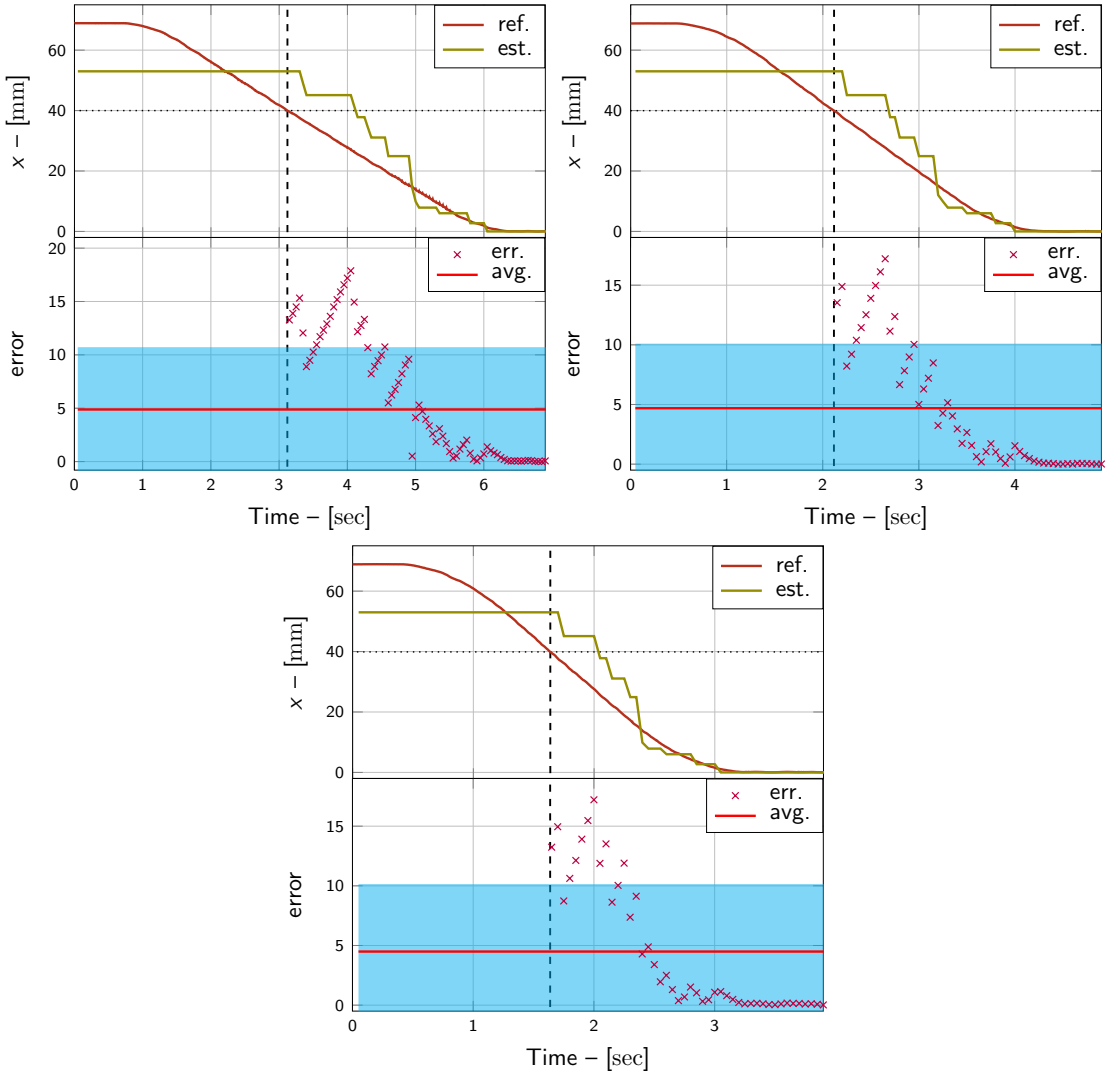

Figure 4.22. In-plane matrix tests (1), (2) and (3): SMACK performs an approaching manoeuvre to the EAU, going from 70 mm to 0 mm in x axis direction. Manoeuvre time is 5 s - 3 s - 2 s.

Measurement along the y direction

To test the estimation along the y axis, six tests are performed. The procedure is conceptually represented in Fig. 4.23 and is as follows:

- SMACK is mounted on the end-effector of the robotic arm and the EAU capture face on the fixed frame;
- A first capture is performed to set motion capture system zero;
- SMACK is then retracted in the $-x$ direction at a fixed distance d, and moved to the initial position in the $-y$ direction;
- SMACK performs a straight line manoeuvre, parallel to the EAU capture face in the y direction from the initial position $-y$ to the final symmetrical position $+y$, with different manoeuvre time whilst the matrix sensor and the motion capture system save the data for post-processing.

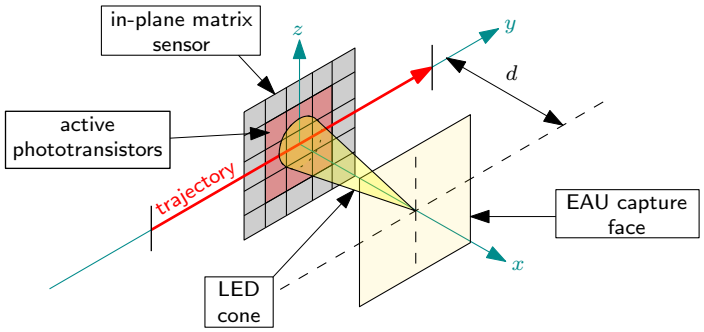

Figure 4.23. Schematic representation of test performed on the in-plane matrix to evaluate in plane position estimation errors.

Test results are reported in Tabs. 4.8 and 4.9 and in Figs. 4.24 and 4.25.

Tests along the z direction are not performed because the matrix has the same response behaviour as in the y direction, since it is symmetric.

The main performance parameters are as follows:

- **Maximum measurement range** $[-15 \div 15]$ mm in both y and z directions.

  In Fig. 4.24 and 4.25, the measurement range is represented with the vertical light red band.

- **Accuracy** 2.5 mm
- **Maximum operating distance** 40 mm

  The operating distance can be extended up to 80 mm with a greater measurement error due to the fact that the power of the beacon decreases.

- **Average error**

  3.11 mm at distance of 10 mm

  6.47 mm at distance of 30 mm

  As visible in Fig. 4.24 and 4.25, the error is calculated within the measurement range (the vertical light red band). The accuracy improves as the distance between the matrix sensor and the LED decreases. The error in estimating in-plane position is within the tolerated misalignment by the gripper (shown in Tab. 4.2).

Test	**Distance**		**Manoeuvre**	**Error**	
ID	x [mm]	y [mm]	**time** [s]	**avg.** [mm]	σ [mm]
4	30	$-30 \div 30$	5	6.56	3.39
5	30	$-30 \div 30$	3	6.46	3.46
6	30	$-30 \div 30$	2	6.39	3.68
			average error	**6.47**	**3.51**

Table 4.8. Values characterizing the straight trajectory along the y axis at a fixed distance of 30 mm from the LED and the resulting estimation errors for the in-plane matrix sensor test.

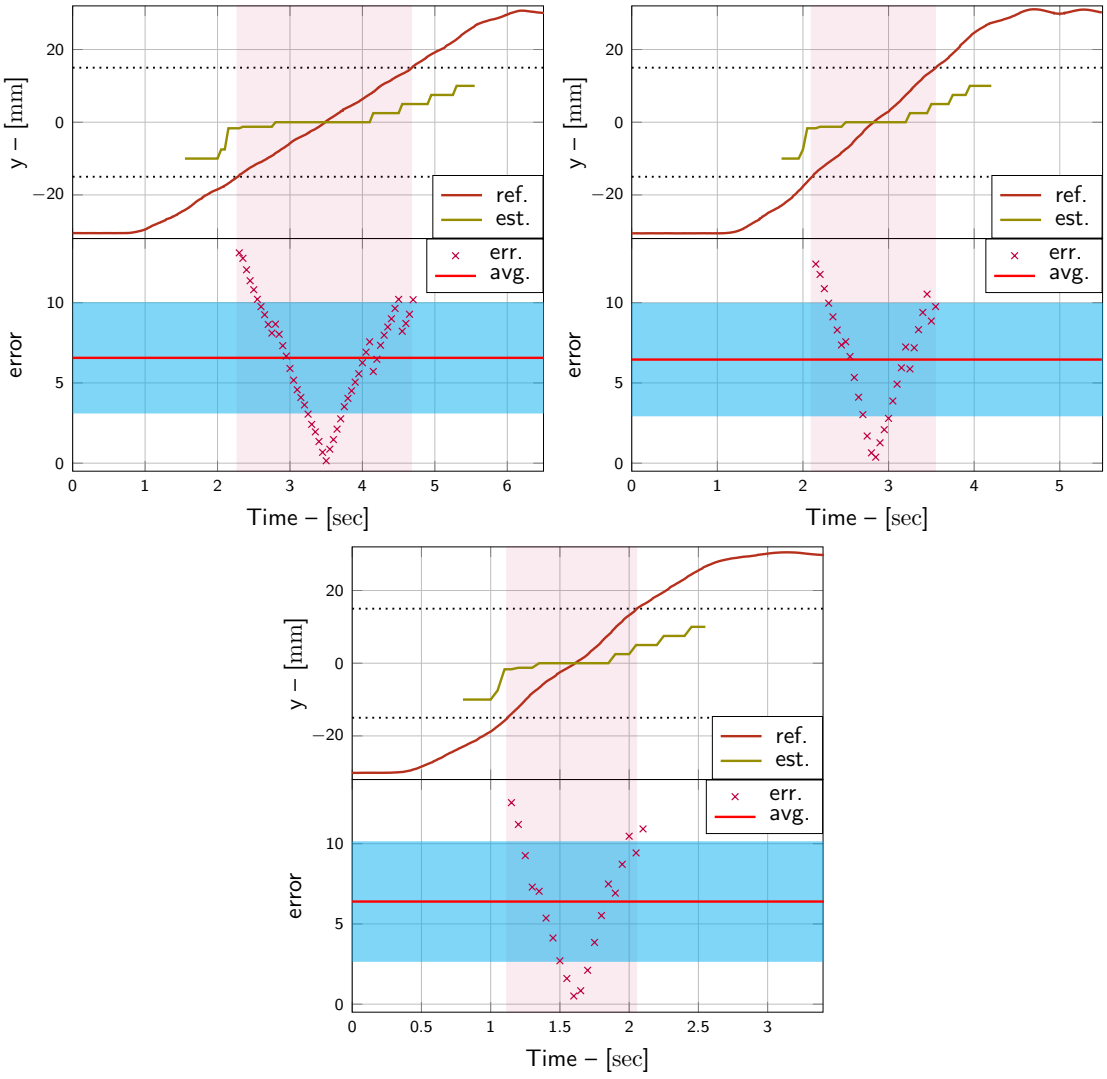

Figure 4.24. In-plane matrix tests (4), (5) and (6): SMACK performs a straight line trajectory going from −30 mm to 30 mm in y axis direction at a constant distance of 30 mm from the EAU capture face. Manoeuvre time is 5 s - 3 s - 2 s.

Test ID	**Distance**		**Manoeuvre time** [s]	**Error**	
	x [mm]	y [mm]		**avg.** [mm]	σ [mm]
7	10	$-20 \div 20$	5	3.13	2.19
8	10	$-20 \div 20$	3	2.94	2.09
9	10	$-20 \div 20$	2	3.27	2.32
			average error	**3.11**	**2.20**

Table 4.9. Values characterizing the straight trajectory along the y axis at a fixed distance of 10 mm from the LED and the resulting estimation errors for the in-plane matrix sensor test.

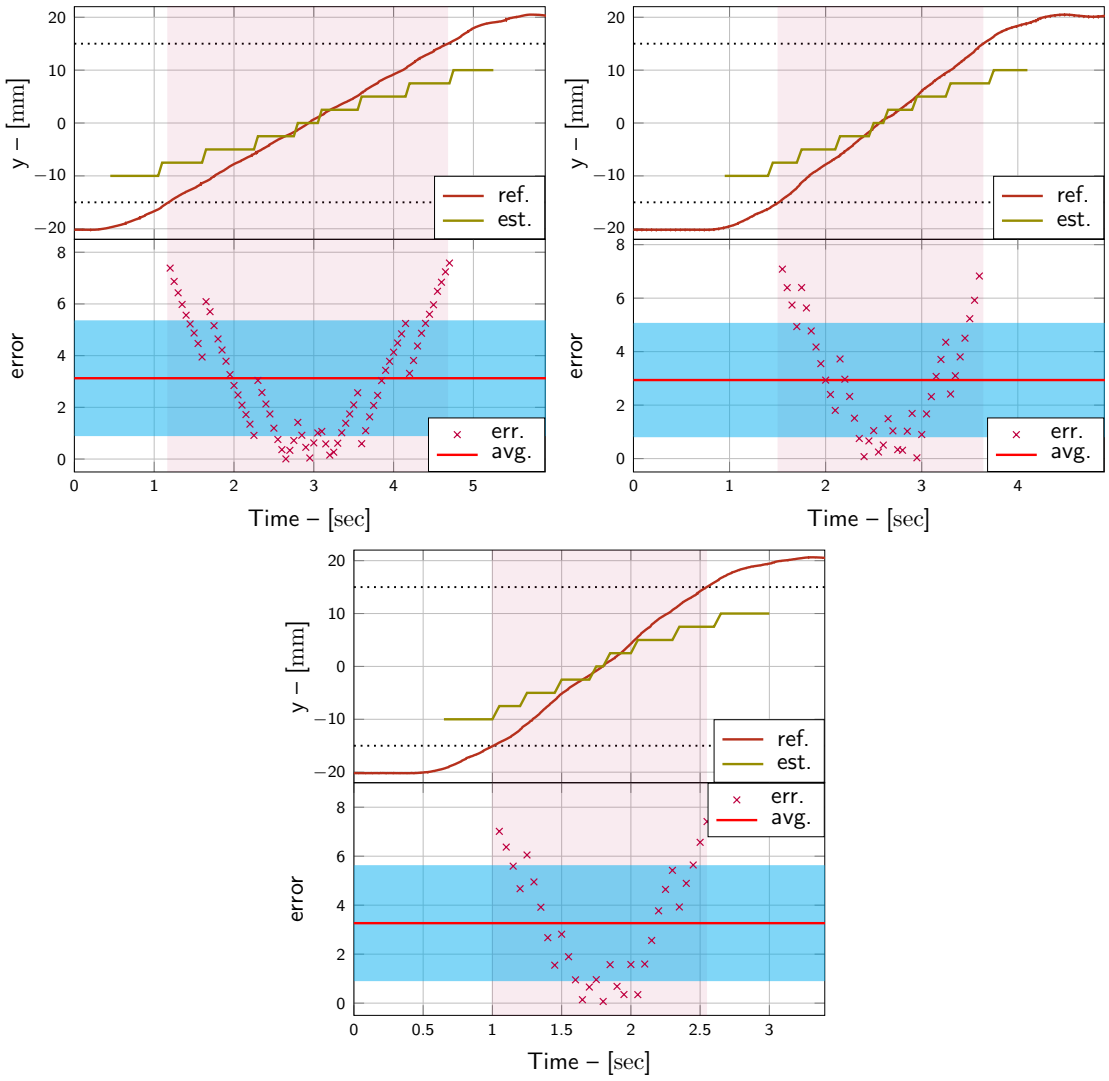

Figure 4.25. In-plane matrix tests (7), (8) and (9): SMACK performs a straight line trajectory going from −20 mm to 20 mm in y axis direction at a constant distance of 10 mm from the EAU capture face. Manoeuvre time is 5 s - 3 s - 2 s.

4.2.4 Roll matrix sensor tests

The roll matrix is able to calculate the roll angle on the basis of the number of phototransistors activated by the LED placed on the EAU capture face. To test its performance, a total of ten tests are performed as follows:

- SMACK is mounted on the end-effector of the robotic arm and the EAU capture face on the fixed frame;
- A first capture is performed to set motion capture system zero;
- SMACK is then retracted in the $-x$ direction at a fixed distance d;
- SMACK performs a rotation manoeuvre around the x axis which takes it from an angle of -15 deg to 15 deg whilst the roll matrix sensor saves the data for post-processing.

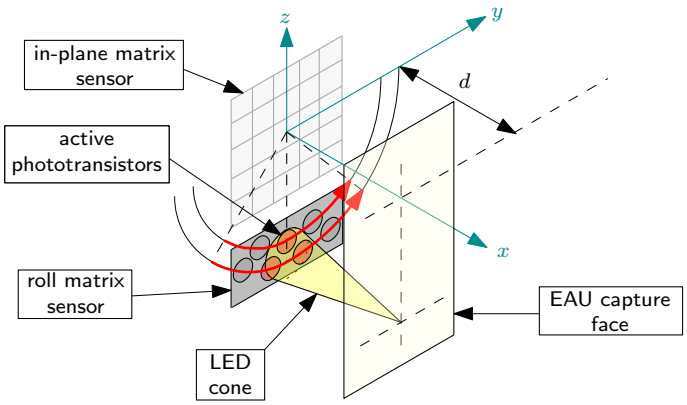

Figure 4.26. Schematic representation of the test performed to establish the performances of the roll matrix sensor.

The results of the tests are reported in Tabs. 4.10 and Figs. 4.27 to 4.36.

These are performed by increasing the distance from the EAU along the x direction. The main performance parameters are as follows:

- **Maximum measurement range** $[-7 \div 7]$ deg

  In Figs. 4.27 to 4.36, the measurement range $[-10.5 \div 10.5]$ deg is represented with the vertical light red band.

- **Accuracy** 1.75 deg

- **Maximum operating distance** 40 mm

  Tests performed at a distance greater than 40 mm show an incorrect reconstruction of the manoeuvre even if the error is comparable to that of the other tests.

- **Average error** 3.12 deg

  As in Figs. 4.27 to 4.36, the error is calculated within the measurement range (the vertical light red band). The error in estimating the roll angle is within the tolerable misalignment by the gripper (shown in Tab. 4.2).

Test ID	**Roll angle** [deg]	**Distance** x [mm]	**Error**	
			avg. [deg]	σ [deg]
1	$-15 \div 15$	10	1.73	1.00
2	$-15 \div 15$	15	2.58	1.45
3	$-15 \div 15$	20	2.93	1.59
4	$-15 \div 15$	25	3.08	2.16
5	$-15 \div 15$	30	3.30	2.40
6	$-15 \div 15$	35	3.86	1.91
7	$-15 \div 15$	40	3.92	2.14
8	$-15 \div 15$	50	3.63	2.37
9	$-15 \div 15$	60	3.28	2.47
10	$-15 \div 15$	70	2.90	1.65
		average error	**3.12**	**1.91**

Table 4.10. Values characterizing the rotation manoeuvre around x and the resulting estimation errors for the roll matrix sensor test.

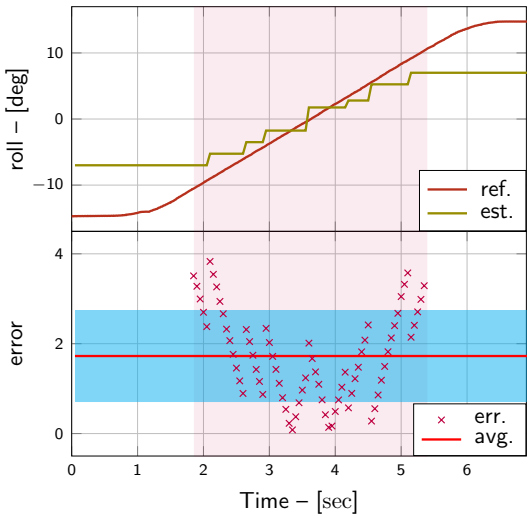

Figure 4.27. Roll matrix test (1): SMACK performs a rotation going from −15 deg to 15 deg around x axis at a distance of 10 mm from the EAU capture face.

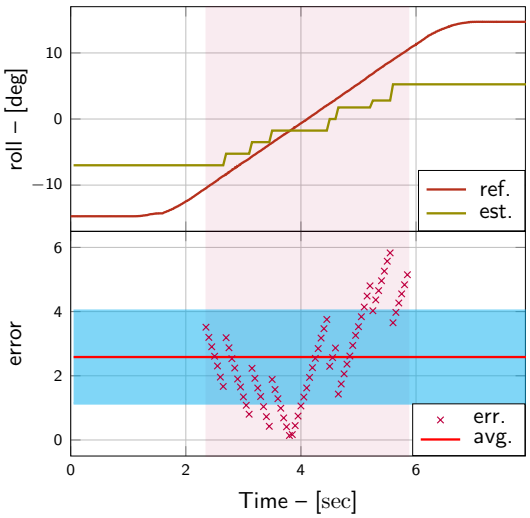

Figure 4.28. Roll matrix test (2). SMACK performs a rotation going from −15 deg to 15 deg around x axis at a distance of 15 mm from the EAU capture face.

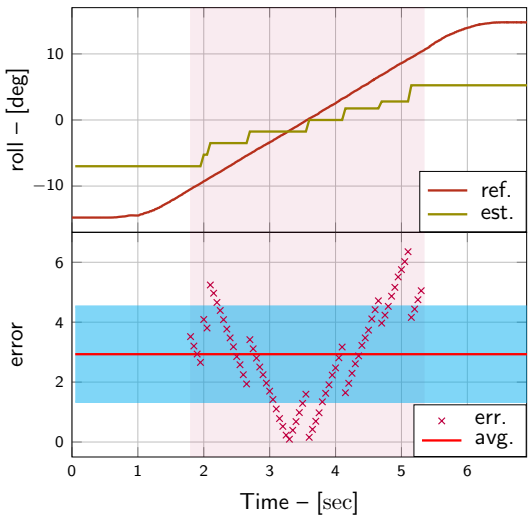

Figure 4.29. Roll matrix test (3): SMACK performs a rotation going from −15 deg to 15 deg around x axis at a distance of 20 mm from the EAU capture face.

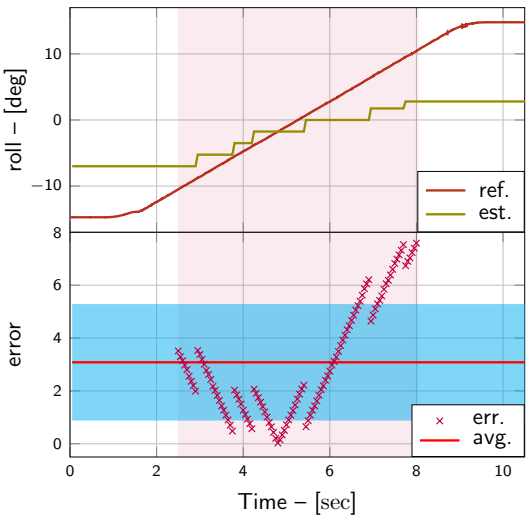

Figure 4.30. Roll matrix test (4). SMACK performs a rotation going from −15 deg to 15 deg around x axis at a distance of 25 mm from the EAU capture face.

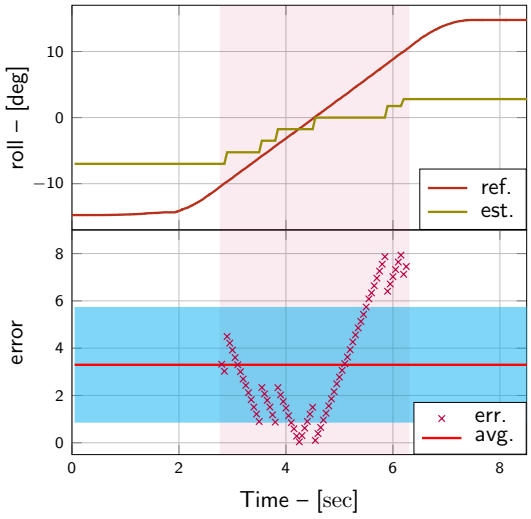

Figure 4.31. Roll matrix test (5): SMACK performs a rotation going from −15 deg to 15 deg around x axis at a distance of 30 mm from the EAU capture face.

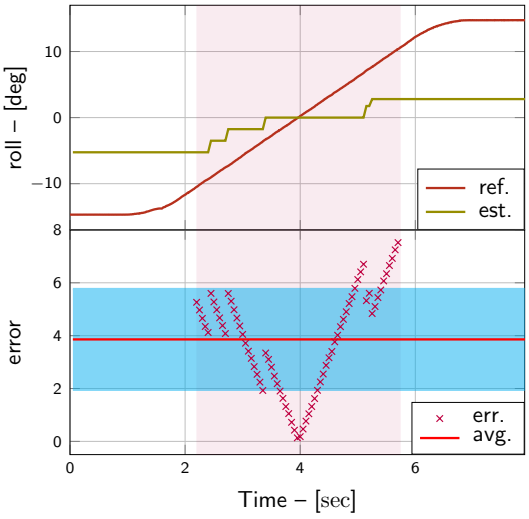

Figure 4.32. Roll matrix test (6). SMACK performs a rotation going from −15 deg to 15 deg around x axis at a distance of 35 mm from the EAU capture face.

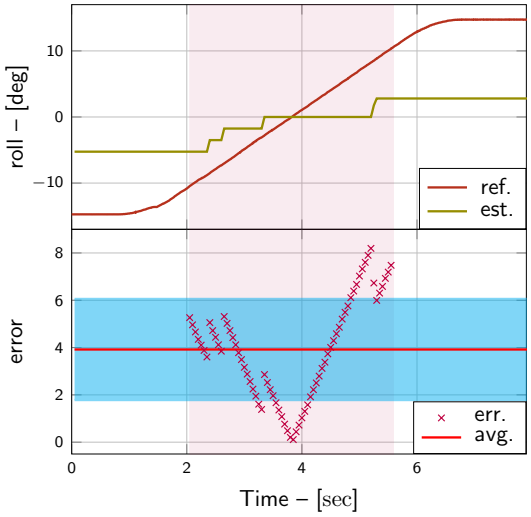

Figure 4.33. Roll matrix test (7): SMACK performs a rotation going from −15 deg to 15 deg around x axis at a distance of 40 mm from the EAU capture face.

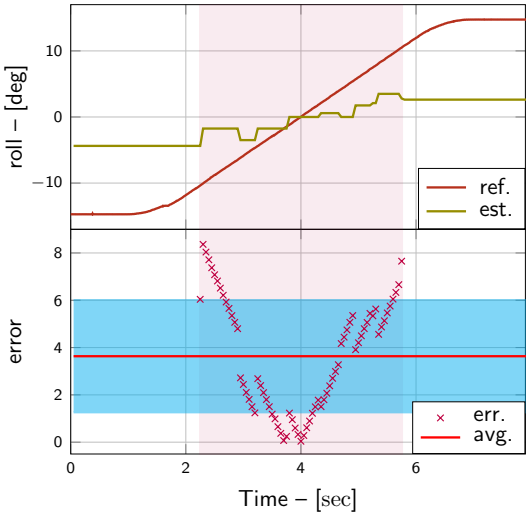

Figure 4.34. Roll matrix test (8). SMACK performs a rotation going from −15 deg to 15 deg around x axis at a distance of 50 mm from the EAU capture face.

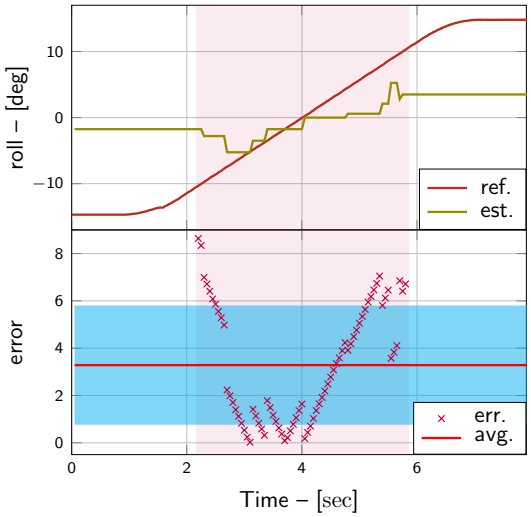

Figure 4.35. Roll matrix test (9): SMACK performs a rotation going from −15 deg to 15 deg around x axis at a distance of 60 mm from the EAU capture face.

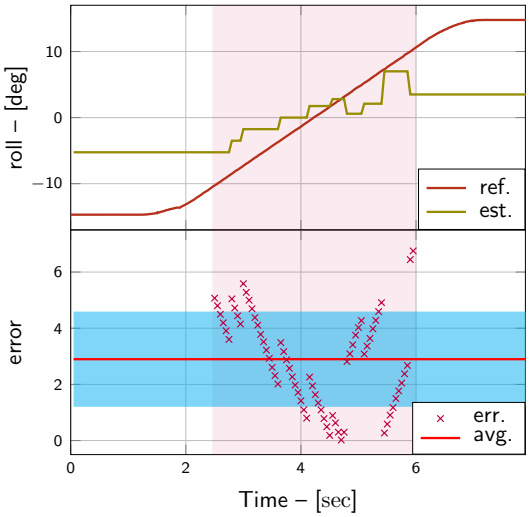

Figure 4.36. Roll matrix test (10). SMACK performs a rotation going from −15 deg to 15 deg around x axis at a distance of 70 mm from the EAU capture face.

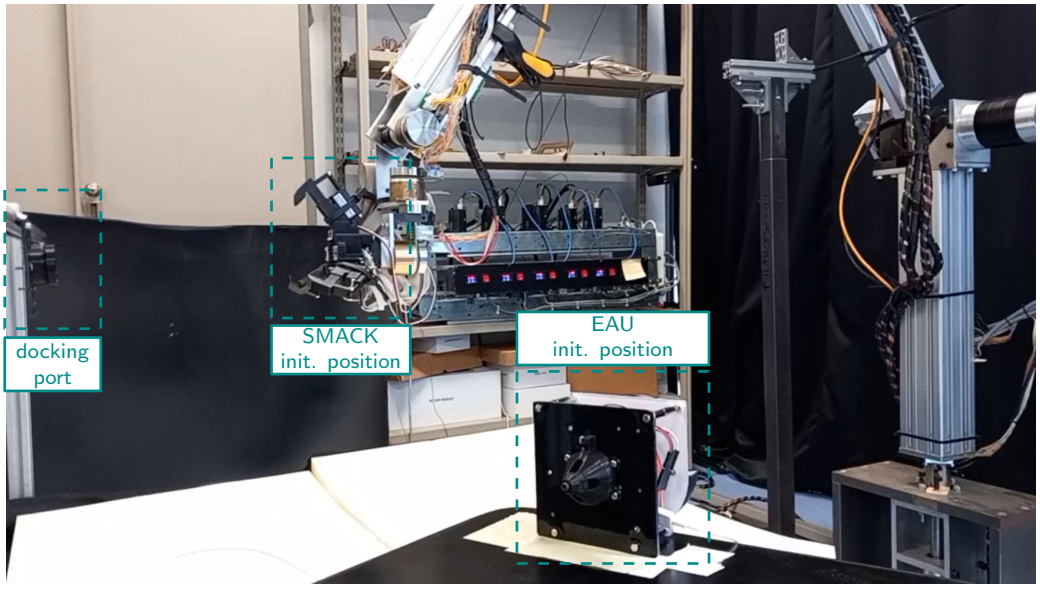

Figure 4.37. Functional system test set-up.

4.3 System level test

4.3.1 Functional system test

After the measurement subsystem tests previously described in Sect. 4.2, the final test was designed to verify the assembly phase. This open-loop test involves the integrated systems but the control loop is not closed trough the navigation algorithm. The aim of this test is to validate system mechanisms.

To execute this test, the set-up is visible in Fig. 4.37 and was as follows:

- SMACK has been mounted on the end-effector of the robotic arm;
- The EAU has been placed in a known position;
- The drogue of the docking port has been mounted on a fixed frame;
- The SMACK computer has been connected to the robotic arm to allow SMACK to transmit the desired position to the robotic arm.

Since this is an open-loop test, the positions of the EAU and of the docking port have been previously hard coded in the algorithm for the test. The algorithm for the assembly procedure provided eight different positions for SMACK, with a manoeuvre velocity of 50 mm/s. Referring to the frames of Fig. 4.38, the eight points are:

1. *Neutral*: position in which SMACK is far from any other object;
2. *Pre-capture*: in front of the EAU and aligned with it, but at a distance of approximately 100 mm;
3. *Capture*: aligned with the EAU, at a distance of few millimeters in order to allow the closure of the fingers and capture the EAU;
4. *Post-capture*: after the capture occurred, SMACK and the EAU have been lifted by 100 mm;
5. *Neutral*;
6. *Pre-docking*: in front of the docking port and aligned with it, but a distance of approximately 100 mm;
7. *Docking*: the position where the docking mechanism can be activated;
8. *Post-docking*: after the assembly, SMACK has been moved to the neutral position.

The test has bee repeated several times and highlighted that:

1. SMACK is able to perform assembly tasks. In particular SMACK is able to capture the EAU, drive the robotic arm to the target and to perform the docking;
2. Some improvements are required for the EAU. In fact, is able to perform the capture but it is not able to force a perfect alignment. As a consequence, the fingers do not match the slot, resulting in a non-nominal capture. This causes the EAU to slighly slip during the post-capture phase and then a non-nominal docking.

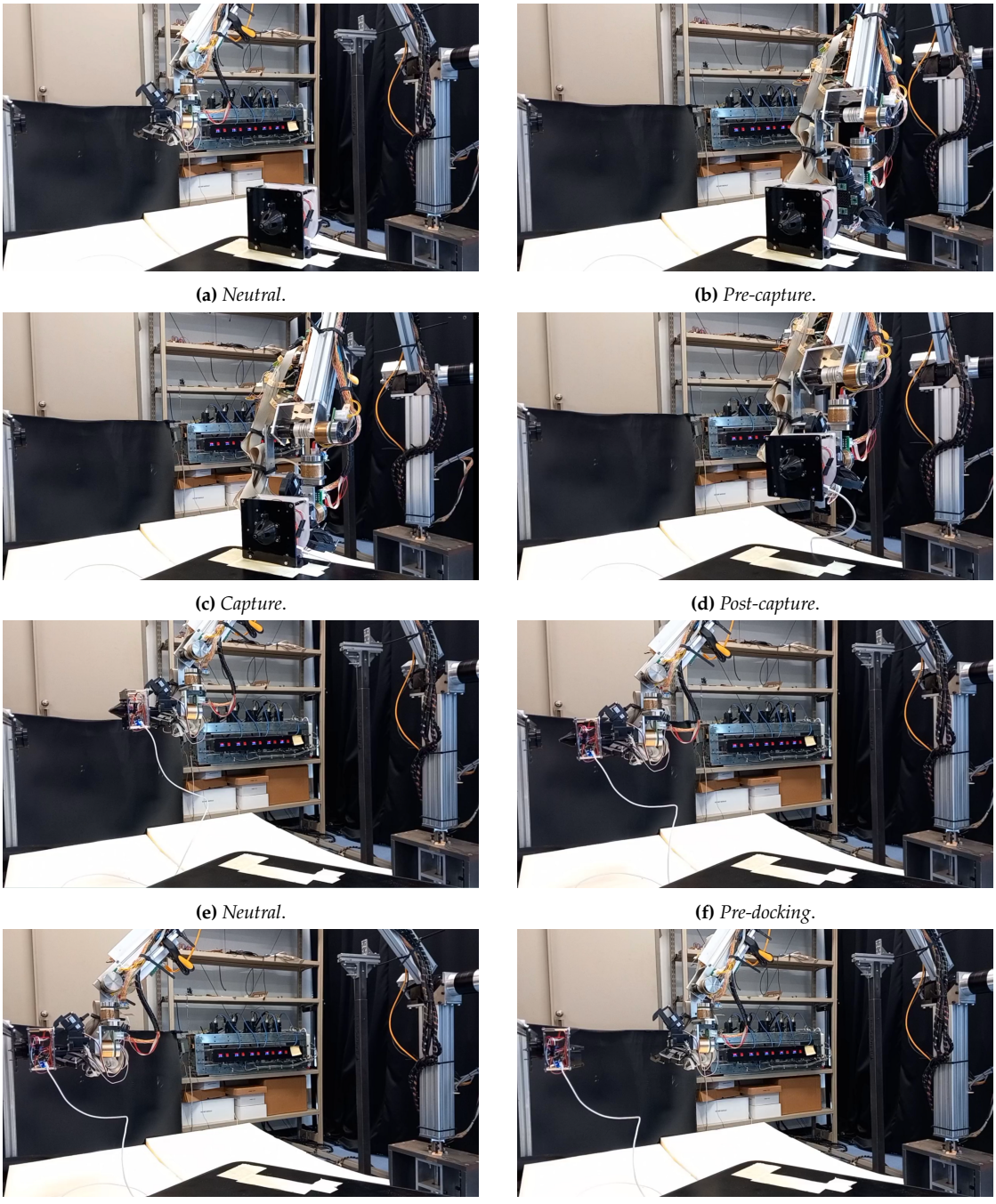

(a) *Neutral*.
(b) *Pre-capture*.
(c) *Capture*.
(d) *Post-capture*.
(e) *Neutral*.
(f) *Pre-docking*.
(g) *Docking*.
(h) *Post-docking*.

Figure 4.38. Video frames of the eight points of the functional system tests.

5

Conclusions and future works

The AUtonomous Technologies for Orbital servicing and Modular Assembly (AUTOMA) project is motivated by the high interest of the space community in the technologies to enable the In-Orbit Assembly missions. The AUTOMA project has the purpose to upgrade a capture tool (SMACK) and develop an assembly unit (EAU) to perform experiments on the IOA.

This work provided an overview of the sensors used by SMACK and their validation, together with the development of the assembly unit.

The work continued the previous developments visible in [2] and can be divided into the following parts:

1. EAU circuit design;
2. Dynamic tests on the three SMACK sensors to verify:
   (a) Their performances under different conditions;
   (b) The performance of the model-based pose estimation algorithm.

   These subsystem tests confirmed that the sensors are able to retrieve the pose of the target and their performance are with an error that is lower than the misalignemnt tolerated by the gripper of SMACK.

   The navigation camera that is used as the first navigation sensor can measure the target pose from 1.2 m to 60 mm. Other sensors are needed to measure the target pose during the final capture phase. These sensors are chosen to be four Time-of-Flight sensors and two matrix sensors made of a pattern of phototransistors.

   The ToF sensors are able to measure both the distance and the pitch and yaw angle (with the respectively rates) and a Kalman filter algorithm

to enhance their estimation has been implemented. They measure the distance and relative attitude from 90 mm up to 30 mm from the EAU capture face.

The dynamic tests performed on ToF sensors and to evaluate the Kalman filter performance report that the estimation errors are approximately of 1.5 mm for distance estimation, and below 2 deg for attitude estimation. These tests also evaluated the ability of the Kalman filter to estimate velocity. The maximum errors are approximately 1.9 mm/s and of 2.5 deg/s in tests where all 3 degrees of freedom are involved. The filter was built on a constant velocity dynamic model. The greatest errors in velocity estimation, in fact, occur in the variable speed phases (acceleration or deceleration of the maneuver performed by SMACK). Furthermore, the slower the maneuver, the smaller the estimation error will be, since it gives the Kalman filter time to converge.

The two matrices are activated by two infra-red LEDs placed on the EAU capture face and are used in the final part of the approach manoeuvre. The 5×5 phototransistor matrix is used to measure the distance in the final 40 mm from the EAU, and is used to measure the in-plane position of the EAU in the final 80 mm. The roll matrix is used to measure the roll angle of the EAU in the final 40 mm from the EAU.

The dynamic tests on the in-plane matrix sensor provided an average error of 4.5 mm in the distance measure and a maximum average error of 6.5 mm for the in-plane position. The tests on the roll matrix sensor provided an average error of 3 deg. It is important to note though that this is an average error, the estimate of distance, in-plane position, and roll angle improve noticeably as SMACK gets to the capture position.

The tolerated misalignments are about 12 mm along y axis, -10 mm to 15 mm along the z axis, 9 deg in rotation around x axis, 5 deg in rotation around y axis, 10 deg in rotation around the z axis, so all the sensors error are within the tolerable zone by the gripper.

3. Open-loop test, which:

   (a) Confirmed the validity of the mechanisms;

   (b) Highlighted some required improvements.

   The improvements concern the capture interfaces and the concave slot design. During the handling, the upper finger slipped in the concavity of the capture interface, resulting in misalignment errors for the docking phase.

5.1 Future work

Numerous tests have dynamically characterised the SMACK sensors. In [2] the guidance algorithm has been validated, so the next steps are devoted to closed-loop tests, in order to perform an autonomous assembly.

Simultaneously with the execution of the tests on SMACK, the development of a floating module for the low-friction table is on-going, which will be used to simulate the free-fall motion of the target satellite, decoupling it from the frictional forces. In the future, it will be interesting to verify the ability of SMACK to capture the EAU from the storage to carry out an assembly on a mobile receiving structure. Furthermore, the capture of a moving target will also be interesting to analyse. This test will evaluate whether SMACK can synchronise with the moving target to capture it.

One open point in the project that has not been explored yet is how SMACK receives information from the assembly unit about the success of the assembly operation.

To summarise, future work will cover the following:

1. Improvement of the slots in the grappling features;
2. Autonomous assembly tests (docking port unable to move and positioned on the low-friction module);
3. Autonomous capture of a moving target on the low-friction table;
4. Study of communication strategies between assembly unit and satellite chaser to transmit successful assembly.

References

[1] Francesco Branz et al. "Miniature docking mechanism for CubeSats". In: *Acta Astronautica* 176 (2020), pp. 510–519. ISSN: 0094-5765. DOI: https://doi.org/10.1016/j.actaastro.2020.06.042.

[2] Alex Caon. "Development of a smart capture system for On-Orbit Servicing with space robots". 2023.

[3] Alex Caon, Francesco Branz, and Alessandro Francesconi. "Characterization of a new positioning sensor for space capture". In: 2021.

[4] Alex Caon, Francesco Branz, and Alessandro Francesconi. "Development and test of a robotic arm for experiments on close proximity operations". In: (2022).

[5] Alex Caon et al. "Ground Facility for Validation of Proximity Operations: a Hardware–In–the–Loop Experiment". In: *2020 IEEE 7th International Workshop on Metrology for AeroSpace (MetroAeroSpace)*. 2020, pp. 555–560. DOI: 10.1109/MetroAeroSpace48742.2020.9160309.

[6] NASA Johnson Space Center. "Reference Guide to the International Space Station". In: *National Aeronautics and Space Admnistration, Houston* (2015).

[7] *ClearSpace website*. The European Space Agency (ESA). URL: https://www.esa.int/Space_Safety/ClearSpace-1.

[8] *Compliant Assistance and Exploration SpAce Robot (CAESAR)*. DLR. URL: https://www.dlr.de/rm/en/desktopdefault.aspx/tabid-13282/#gallery/32048.

[9] *CONFERS On-Orbit Servicing (OOS) Mission Phases*. The Consortium for Execution of Rendezvous and Servicing Operations (CONFERS). 2022.

[10] XiLun Ding et al. "A review of structures, verification, and calibration technologies of space robotic systems for on-orbit servicing". In: *Science China Technological Sciences* 64.3 (2021), pp. 462–480.

[11] *Enabling science through new technologies*. NASA. URL: https://hubblesite.org/mission-and-telescope/servicing-missions.

[12] Bernard Friedland. *Control system design: an introduction to state-space methods*. Courier Corporation, 2012.

[13] *In space manufacturing and assembly (ISMA)*. Airbus. URL: https://www.airbus.com/en/newsroom/news/2022-05-in-space-manufacturing-and-assembly.

[14] *Mission Extension Vehicle (MEV)*. URL: https://www.northropgrumman.com/space/space-logistics-services/.

[15] *On-Orbit Servicing, Assembly, and Manufacturing 1 (OSAM-1)*. URL: https://nexis.gsfc.nasa.gov/OSAM-1.html.

[16] *On-Orbit Servicing, Assembly, and Manufacturing 2 (OSAM-2)*. URL: https://www.nasa.gov/mission_pages/tdm/osam-2.html.

[17] *Phoenix program*. Defense Advanced Research Projects Agency (DARPA). URL: https://www.darpa.mil/program/phoenix.

[18] Danielle Piskorz and Karen L Jones. "On-orbit assembly of space assets: A path to affordable and adaptable space infrastructure". In: *The Aerospace Corporation* (2018).

[19] D Reintsema et al. "DEOS - the German robotics approach to secure and de-orbit malfunctioned satellites from low earth orbits". In: Japan Aerospace Exploration Agency (JAXA) Japan. 2010, pp. 244–251.

[20] Francesco Sansone, Francesco Branz, and Alessandro Francesconi. "A relative navigation sensor for CubeSats based on LED fiducial markers". In: *Acta Astronautica* 146 (2018), pp. 206–215. ISSN: 0094-5765. DOI: https://doi.org/10.1016/j.actaastro.2018.02.028.

[21] Andrew Tatsch, Norman Fitz-Coy, and Svetlana Gladun. "On-orbit servicing: A brief survey". In: *Proceedings of the IEEE International Workshop on Safety, Security, and Rescue Robotics (SSRR'06)*. 2006, pp. 276–281.

Acknowledgments

I ringraziamenti nella tesi di laurea possono sembrare la formalità di uno dei molti traguardi che si raggiungono nell'arco della vita, ma non voglio perdere un'occasione per essere grata e non darò per scontato tutto l'affetto e il supporto che ho ricevuto in questi anni. Ci sono molte persone che vorrei ringraziare, persone senza la quale questo lavoro e traguardo non sarebbero mai stati possibili.

Dal punto di vista accademico, vorrei ringraziare il Dott. Francesco Branz che mi ha permesso di lavorare a questo progetto.

Vorrei dire grazie ad Alex, che mi ha seguita e supportata (ma soprattutto sopportata) durante tutti questi mesi. Non avrei mai potuto immaginare che avrei imparato così tanto e farlo divertendomi. La tua passione e la tua conoscenza mi hanno ispirata immensamente, e hai riacceso in me la speranza e dissipato i dubbi sul mio posto nel mondo. In te ho trovato un mentore e vorrei essere per gli altri quello che tu sei stato per me. Grazie, detto con tutto l'affetto e la stima di cui sono capace, e grazie soprattutto per tutti i ravioli.

A Federico e Luca, grazie per avermi accolta tra voi in laboratorio e avermi fatta sentire parte del gruppo dal primo istante.

Ad Alessandra, Nicola, Simone, Alessandro, Brunella, Martina. I miei colleghi e compagni di viaggio. Grazie per tutti questi anni di risate e disagio condiviso. Siete gli amici che sono sicura non perderò ora che lascio indietro un pezzo di vita. E diciamoci la verità, senza di voi sarei ancora persa a preparare l'esame di Algebra.

A Walter, che durante tutti questi anni si è preso cura della mia cattiva postura causata dalle interminabili ore passate seduta a studiare.

Agli amici della palestra, che letteralmente come una "Manna dal cielo" sono entrati nella mia vita all'improvviso e vi rimarranno per sempre. Tutti i giorni mi fate sentire essenziale, e non c'è sensazione più incredibile da provare. Da oggi non avrò più scuse per arrivare tardi in palestra.

Al team di League of Legends, la più bella cosa capitata con la pandemia.

Grazie per tutte le risate, e per aver curato la mia salute mentale ad ogni partita fatta assieme.

Ad Elena e Francesca, le amiche a cui voglio un mondo di bene senza averglielo mai detto. Grazie di tutto il supporto e per aver sopportato la mia assenza, senza farmelo pesare nemmeno per un secondo.

A Cy e Sano, che sono come fratelli (anche se sappiamo che non sono ancora nessuno). Grazie per tutti i momenti di spensieratezza passati insieme.

Alla mia famiglia, al mio papà, alla mia mamma e al mio fratellone. Mi avete supportata ed ispirata con il vostro esempio ogni giorno. Vi ho sottoposti al mio pessimo carattere ma voi siete sempre lì, ogni giorno, ad alleggerirmi l'anima e a farmi sentire che tutto è possibile.

Ai miei cugini Alessia ed Enrico, siete le mie fondamenta e avete contribuito a rendermi la persona che sono.

E infine a Stefano, il mio Nord celeste, il mio migliore amico. Sei la mia quotidiana iniezione di bellezza, fiducia ed entusiasmo. Da ora possiamo, e non vedo l'ora, iniziare a costruire la nostra vita assieme.

Tutti voi avete creduto in me più di quanto io non abbia mai fatto. Ogni vostra parola di incoraggiamento e di affetto ha lasciato un segno profondo. Questo traguardo lo dedico a voi, che siete le persone più importanti della mia vita.

Martina Imperatrice, 13 Aprile 2023

List of Figures

List of Tables